DFT Study of Sorption of Palladium onto Montmorillonite in a Saline Environment

DFT STUDY OF SORPTION OF PALLADIUM ONTO MONTMORILLONITE IN A SALINE ENVIRONMENT

By

KEFEI LIU, B.ENG

A THESIS

SUBMITTED TO THE DEPARTMENT OF ENGINEERING PHYSICS

AND THE SCHOOL OF GRADUATE STUDIES

OF MCMASTER UNIVERSITY

IN PARTIAL FULFILLMENT OF THE REQUIREMENTS

FOR THE DEGREE OF

MASTER OF APPLIED SCIENCE

Master of Applied Science (2024) McMaster University

(Engineering Physics) Hamilton, Ontario, Canada

TITLE: DFT Study of Sorption of Palladium onto Montmorillonite in a Saline Environment

AUTHOR: Kefei Liu

B.Eng. (Engineering Physics)

McMaster University, Hamilton, Canada

SUPERVISOR: Dr. Shinya Nagasaki

NUMBER OF PAGES: lxviii, 68

For all those who have helped me throughout my study

Abstract

Palladium-107 is one of the radionuclides of interest for the safety assessment of deep geological disposal of used nuclear fuel. Bentonite clay is used in the engineered barrier system of a deep geological repository for used nuclear fuel because of its low permeability, large swelling capacity, retention properties and thermal stability. With montmorillonite being the main component of the bentonite clay, this study focuses on using the Density Functional Theory (DFT) simulation to explore the sorption mechanism of palladium on montmorillonite in a Na-Ca-Cl saline environment. The method of substituting Se(IV) species with Pd species and phlogopite edge surfaces with the basal and edge surfaces of montmorillonite is justified with benchmark simulation results. The presence of $PdCl^{+}$, $PdCl_2$, $PdCl_3^{-}$, and $PdCl_4^{2-}$ complexes in the Na-Ca-Cl saline environment is confirmed by the calculated negative free energy. The most favourable palladium chloride species for sorption reactions onto montmorillonite in the saline environment is $PdCl_4^{2-}$, followed by $PdCl_3^{-}$, $PdCl_2$ and $PdCl^{+}$.

Acknowledgements

I would like to thank my supervisor, Dr. Shinya Nagasaki, and our collaborating researcher, Dr. Satoru Tsushima, for all of their guidance and help throughout my study at McMaster. I would also like to thank my colleagues, Dr. Zhiwei Zheng, Jianan Liu, and Jieci Yang, for all their helpful discussions and support throughout my research. Finally, I would also like to thank my parents for their continued support throughout my study.

I would also like to thank Tammy Yang from the Nuclear Waste Management Organization for reviewing conference papers, as well as this thesis, and providing helpful comments.

This research was funded by the NWMO and the Natural Sciences and Engineering Research Council of Canada.

Abbreviations

Al	Aluminum
CANDU	CANada Deuterium Uranium
CASTEP	CAmbridge Serial Total Energy Package
DFT	Density Functional Theory
DGR	Deep Geological Repository
H	Hydrogen
K	Potassium
Mg	Magnesium
Na	Sodium
NWMO	Nuclear Waste Management Organization
O	Oxygen
Pd	Palladium
Si	Silicon

Nomenclature

$E_{sorption}$	Sorption energy
$E_{absorbent}$	Energy of the absorbent
$E_{solvent}$	Energy of the solvent
$E_{solution}$	Energy of the solution
$E[\rho]$	Total energy functional
$\hbar$	Reduced planck's constant
$T[\rho]$	Kinetic energy functional
$V_{ext}[\rho]$	External potential energy functional
$V_{ee}[\rho]$	Electron-electron interaction energy functional
$\rho(\mathbf{r})$	Electron density
ρ_0	Ground state electron density
E_0	Ground state energy
$\psi_i(\mathbf{r})$	Kohn-Sham orbitals
E_{XC}^{LDA}	Local Density Approximation of the correlation-exchange energy
E_{XC}^{GGA}	General Gradient Approximation of the correlation-exchange energy

Contents

List of Tables

List of Figures

1. Introduction

1.1 Background

Fission is a nuclear process where a heavy atomic nucleus splits into two smaller nuclei along with a few neutrons and a large amount of energy. This reaction typically occurs when a heavy nucleus, such as uranium-235 or plutonium-239, absorbs a neutron, becomes unstable, and divides into two smaller nuclei. The fission process releases significant energy primarily in the form of kinetic energy of the fragments and as gamma radiation. This energy is harnessed in nuclear reactors for electricity generation. The additional neutrons released can further induce fission in other nuclei, leading to a chain reaction, which is controlled in reactors to maintain a steady release of energy (Knief, 2014).

CANDU (CANada Deuterium Uranium) reactors are a type of nuclear reactor developed in Canada that utilizes natural uranium as fuel and heavy water (Deuterium Oxide, D_2O) as both a moderator and coolant. The use of heavy water allows CANDU reactors to efficiently use natural uranium without requiring enrichment, which reduces fuel costs and increases fuel availability. A distinctive feature of CANDU reactors is their use of horizontal pressure tubes, which house the fuel bundles and allow for on-power refueling, meaning the reactor can continue operating while being refueled. This design enhances operational efficiency and flexibility (Hastings et al., 2018). Additionally, CANDU reactors

have robust safety systems and a unique capability to use alternative fuel cycles, including thorium and recycled uranium, which further distinguishes them from other reactor types (IAEA, 2003).

Nuclear waste is produced during the operation of nuclear reactors, primarily from the fission process. As nuclear fuel, such as uranium or plutonium, undergoes fission, it breaks down into smaller, radioactive fission products. Over time, these fission products accumulate in the fuel, decreasing its efficiency and necessitating its replacement. Spent nuclear fuel is highly radioactive and contains a complex mixture of fission products, transuranic elements (elements heavier than uranium formed by neutron capture), and unused uranium or plutonium. The management of nuclear waste involves careful handling, storage, and eventual disposal to protect human health and the environment. High-level waste (HLW), which includes spent nuclear fuel, requires particularly stringent measures due to its long-lived radioactivity and heat generation (Ewing, 2015).

As of mid-2023, Canada has accumulated approximately 3.3 million used nuclear fuel bundles. This inventory is expected to increase significantly, reaching around 5.6 million bundles by the end of the operational life of the current nuclear reactors. Each year, approximately 90,000 new bundles are generated. This projection takes into account the ongoing operation of the existing fleet of nuclear reactors in Canada. By 2050, the total inventory of used nuclear fuel is expected to reach approximately 5.6 million bundles. This projection is based on current reactor operation timelines and does not account for potential new reactors or the extension of current reactor lifespans beyond their planned operational periods (NWMO, 2022).

The used nuclear fuel is currently stored in licensed facilities at various reactor sites across Canada. These facilities employ both wet and dry storage methods. Wet storage involves placing the used fuel bundles in pools of water, which cools and shields the radiation. Dry storage, which has become more prevalent, involves placing the used fuel in robust, reinforced concrete containers. These dry storage systems are designed to safely contain the radiation and prevent the release of radioactive materials into the environment (NWMO, 2022).

CANDU reactor used nuclear fuel comprises various components resulting from the fission process and neutron capture. The main constituents include fission products, such as cesium-137, strontium-90, and iodine-131, which are highly radioactive. Additionally, the spent fuel contains transuranic elements like plutonium-239, americium-241, and neptunium-237, formed by the absorption of neutrons by uranium-238 in the fuel. There are also residual amounts of uranium-238 and a small fraction of uranium-235 that did not undergo fission. These components make the used fuel highly radioactive and necessitate secure storage and management strategies to mitigate potential environmental and health risks (Hastings et al., 2018; IAEA, 2003).

During the fission process, neutron-rich fission fragments such as silver-107 can be produced. Silver-107 is unstable and decays via beta decay to form palladium-107. The beta decay process involves the transformation of a neutron into a proton, with the emission of a beta particle (electron) and an antineutrino. Another pathway for the formation of palladium-107 involves neutron capture reactions followed by beta decay. For instance, palladium-106 can capture a neutron to form palladium-107 directly. However, this is less common compared to the direct fission product formation and subsequent beta decay.

Fission products may be present in the fuel as volatiles (i.e., iodine, bromine, cesium, rubidium, tellurium), metallic precipitates (i.e., molybdenum, technetium, ruthenium, rhodium, palladium, silver, cadmium, indium, tin, antimony, tellurium), secondary oxide precipitates (i.e., rubidium, cesium, strontium, barium, zirconium, niobium, molybdenum, tellurium), or the soluble oxides in the UO_2 fluorite matrix (i.e., cesium, niobium, tellurium, yttrium, zirconium, the earth alkaline elements strontium, barium, radium and the lanthanides lanthanum, cerium, praseodymium, neodymium, promethium, samarium, europium) (Metz et al., 2012). It is very difficult to conduct post-closure safety assessments due to the complicated chemistry of the used nuclear fuel.

In Canada, the NWMO is responsible for the safe, long-term management of Canada's used nuclear fuel. It features a Deep Geological Repository (DGR) that will safely isolate and contain Canada's used nuclear fuel over the long-term. A DGR is an engineered underground facility designed for the safe and long-term disposal of used nuclear fuel. The primary purpose of a DGR is to contain and isolate radioactive waste from the biosphere for extremely long periods, potentially up to hundreds of thousands of years. This will ensure that the radioactivity of nuclear waste will decay to safe levels before any potential exposure

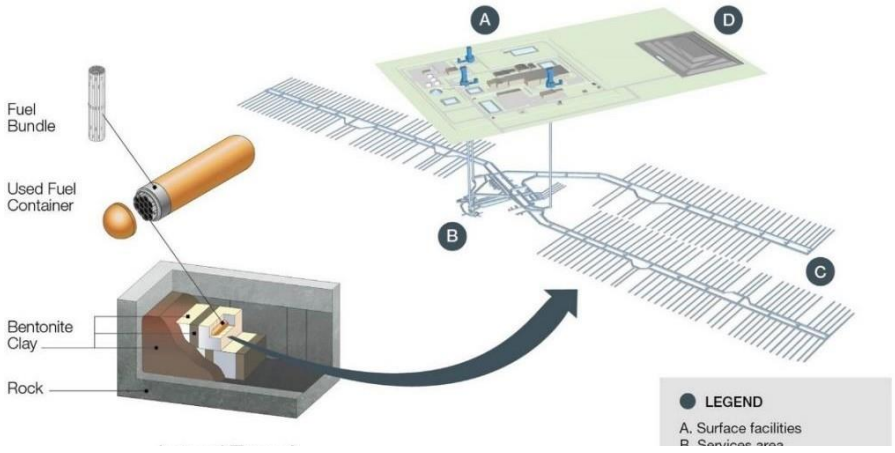

Figure 1: The conceptual design of a DGR (Naserifard, 2021)

to humans or the environment. A conceptual design of a DGR is shown in Figure 1 (Naserifard, 2021).

The repository design includes multiple engineered barriers to prevent any potential release of radioactivity from the nuclear waste. The used fuel bundle is placed in the used fuel container made of steel with a corrosion-resistant copper coating. Containers are then surrounded by buffer material (such as bentonite clay, the main component of which is montmorillonite) (Adams & Williams, 2005) that provides additional containment. The surrounding geological formation provides the final barrier, further isolating the waste from the environment.

Bentonite clay is a type of absorbent aluminum phyllosilicate clay primarily composed of montmorillonite. Formed from volcanic ash, bentonite is renowned for its high cation exchange capacity, significant swelling properties, and ability to absorb water and organic substances.

Bentonite clay possesses several key properties that contribute to its wide usage. Its high cation exchange capacity allows it to bind positively charged ions, such as heavy metals, which can be beneficial in environmental remediation (Churchman, 2002). The clay's swelling ability is attributed to the presence of montmorillonite, which expands when it absorbs water, creating a gel-like consistency that enhances its sealing and buffering capabilities. Additionally, bentonite clay exhibits low permeability, high plasticity, and thermal stability, making it suitable for numerous applications (Murray, 2007).

One of the primary applications of bentonite clay is as a buffer material in geological repositories for the disposal of radioactive waste. Its unique properties make it an ideal

barrier to prevent the migration of radionuclides into the environment. The swelling capacity of bentonite ensures that it can fill gaps and fractures in the repository, providing a tight seal that minimizes the movement of contaminants (Pusch, 2001). Furthermore, its low permeability reduces the flow of water, thereby limiting the transport of dissolved radionuclides. The thermal stability of bentonite also ensures that it can withstand the heat generated by the radioactive waste without significant degradation of its properties (Karnland, 2010).

Palladium-107 is one of the radionuclides of interest for the post-closure safety assessment of deep geological disposal of used nuclear fuel. Na-Ca-Cl and Ca-Na-Cl saline solutions have been observed in Canadian sedimentary and crystalline rocks at repository depths, respectively (NWMO, 2017; NWMO, 2018).

Sorption is a key mechanism for retaining radioactive isotopes because it immobilizes these contaminants, significantly reducing their mobility and preventing their spread through the environment (Nagasaki & Nakayama, 2015). There are few studies on sorption of Pd on montmorillonite in a saline solution. Furthermore, there is not enough information about sorption sites and sorption mechanisms of palladium sorption on montmorillonite when interpreting sorption experimental data. The density functional theory (DFT) calculation would be a very useful molecular modelling method to study the sorption mechanisms of palladium species onto montmorillonite on an atomic scale. DFT offers the capability to study sorption mechanisms at an atomic level, overcoming limitations posed by low solubility from using spectroscopic methods.

1.2 Literature Review

1.2.1 Review of Sorption Experiments

Research on the sorption mechanism of palladium (Pd) onto montmorillonite has revealed several key insights into the interactions between Pd ions and this clay mineral. Montmorillonite's high surface area and cation exchange capacity make it an effective sorbent for various noble metals, including palladium. The primary mechanisms for palladium sorption on montmorillonite include ion exchange, where palladium ions replace exchangeable cations in the interlayer spaces, and surface complexation, where palladium ions form complexes with functional groups on the clay surface. Precipitation of Pd hydroxides on the montmorillonite surface can also occur, especially at higher pH levels (Li et al., 2013; Chutia et al., 2009).

The sorption of palladium onto montmorillonite is influenced by factors such as pH, ionic strength, contact time, and palladium concentration. Higher pH levels generally increase sorption capacity due to reduced competition from H^+ ions and potential formation of $Pd(OH)_2$ precipitates. Increased ionic strength can reduce sorption capacity by competing for exchange sites. Longer contact times enhance sorption capacity, allowing more thorough interaction between palladium ions and montmorillonite (Sharma et al., 2017; Van et al., 2001).

In saline environments, where chloride ions are abundant, palladium ions form various palladium chloride complexes such as $PdCl_4^{2-}$, $PdCl_3^-$, and $PdCl_2$. The formation of these complexes significantly influences the behaviour of palladium, making it less likely to interact directly with sorption sites on montmorillonite. This reduced interaction leads to decreased

sorption capacity in saline conditions due to the stability and mobility of the palladium-chloride complexes (Clever & Johnston, 1979; Kragten, 1980; Ma et al., 2010).

Study of the sorption of palladium onto montmorillonite under conditions of high salinity, elevated pressures, and elevated temperatures will be useful for the understanding of Pd sorption behaviour under repository conditions. Ion exchange and surface complexation are the primary sorption mechanisms, but high chloride concentrations will promote the formation of palladium-chloride complexes, reducing the availability of free Pd ions in solution for sorption. Geochemical modeling studies, such as those by Bradbury and Baeyens (2005), predict palladium speciation under various conditions, highlighting the importance of pH and chloride concentration in determining sorption behaviour. Experimental studies, including batch sorption experiments, provide empirical data on sorption capacities and kinetics, demonstrating the impact of competing ions and elevated temperatures and pressures on the sorption process (Choppin et al., 2002; Wieland et al., 2006).

Experiments conducted by Goguen et al. (2021) provide data on the effect of ionic strength and pH on the sorption process of Pd onto commercial brand MX-80 bentonite. Pd sorption onto MX-80 bentonite decreases with increasing ionic strength. Higher background electrolyte concentrations reduce the sorption capacity of Pd(II), likely due to increased competition for sorption sites. The sorption distribution coefficient (R_d) values for Pd(II) on MX-80 bentonite increase with pH up to a certain point and then stabilize. At lower ionic strengths (IS = 0.01 M), the R_d values are initially higher and become pH-independent at higher pH values. For IS ≥ 0.1 M, the R_d values increase with conditional pH (pH_c), which takes into account the effect of ionic strength, temperature, and ions present in the solution, and then stabilize. The

experiments also show that sorption equilibrium is reached within 7 to 14 days for MX-80 bentonite. Sorption increases between 2 and 7 days and stabilizes thereafter, indicating that a duration of at least 7 days is necessary to ensure equilibrium in sorption studies (Goguen et al., 2021). Additionally, the sorption reaction between the specific $PdCl_4^{2-}$ species and MX-80 was found to be the only reaction that contributes to the sorption process.

In the study from Nagasaki et al. (2019), experiments were conducted using MX-80 bentonite and Na-Ca-ClO_4 solutions with varying ionic strengths (0.1 M, 1 M, 2 M, and 4 M) and pH values (3 to 9). The initial experiments confirmed that Pd sorption on MX-80 in Na-Ca-ClO_4 solutions could be effectively modeled using a two-site protolysis non-electrostatic surface complexation and cation exchange (2SPNE SC/CE) model. When investigating sorption in Na-Ca-Cl-ClO_4 solutions, it was found that the sorption behaviour could only be accurately simulated by including a ternary surface complexation reaction ($S\text{-}OH + Pd_2^{+} + 4Cl^{-} \longleftrightarrow S\text{-}OPdCl_4^{3-} + H^{+}$). This indicated that other potential ternary surface complexations involving different numbers of chloride ions were not significant under the conditions studied. Spectrophotometric measurements taken by Sundaram & Sandell (1955) also demonstrated the formation of palladium-chloride complexes, namely $PdCl^{+}$, $PdCl_2$, $PdCl_3^{-}$, and $PdCl_4^{-}$. There are more probable complexes, but they were much more strongly dissociated with the four main complexes.

Despite finding the only reaction that contribute to the sorption process between palladium-chloride species and montmorillonite, the relationship between the sorption energy of different palladium-chloride species and different sorption sites on montmorillonite remains

uncertain. There is not enough information about sorption sites and mechanisms of palladium sorption when interpreting the data obtained from experiments.

1.2.2 Review of Molecular Modelling Methods

Research on the sorption of heavy metal ions on solid surfaces using DFT encompasses various materials such as graphene, graphene oxide, Carbon NanoTubes (CNTs), metal oxides, and zeolites. Graphene and its derivatives, especially Graphene Oxide (GO), are extensively studied for their high surface area and tunable properties. For instance, Zhao et al. (2011) used DFT to investigate the adsorption of Pb^{2+}, Cd^{2+}, and Hg^{2+} on GO, finding that oxygen-containing functional groups significantly enhance adsorption capacity due to strong interactions with epoxy and hydroxyl groups on GO surfaces (Zhao et al., 2011). Similarly, CNTs, both pristine and functionalized, have been explored for their sorption capabilities. Lu et al. (2006) discovered that functionalization with carboxyl groups improves the sorption capacity of CNTs for Pb^{2+} and Cd^{2+}, as these groups provide stronger binding energies and more favourable adsorption configurations (Lu et al., 2006).

Metal oxides and hydroxides are also effective sorbents for heavy metals. A study by Li et al. (2012) on the adsorption of Hg^{2+} on TiO_2 surfaces using DFT highlighted the role of surface hydroxyl groups in enhancing the adsorption process, providing detailed insights into the atomic-level mechanisms (Li et al., 2012). Additionally, zeolites and clay minerals are widely investigated for their ion-exchange capacities and large surface areas. Park et al. (2010) applied DFT to study the adsorption of Pb^{2+} and Cd^{2+} on zeolite frameworks, demonstrating that metal

ions preferentially adsorb at sites with high aluminum content, and the ion-exchange process is energetically favourable (Park et al., 2010).

Cadmium has similar chemical behaviours as palladium since they are both transition metals in the periodic table. The sorption mechanism of cadmium on montmorillonite surfaces was researched by Du et al. (2022) using both DFT calculations and molecular dynamics (MD) simulations. The research investigated both the (001) and (010) surfaces of montmorillonite. On the (001) surface, Cd^{2+} was sorbed at the center of a silicon-oxygen ring by electrostatic interactions. On the (010) surface, covalent bonds between Cd^{2+} and O was formed for the sorption reaction (Du et al., 2022).

Despite having various studies on heavy metal ion sorption onto solid surfaces, and sorption of elements with similar chemical behaviours with palladium on various surfaces, and DFT being a great molecular modelling method to study sorption mechanisms, there is no studies focusing on the sorption process between palladium species forming complexes with chloride ions and montmorillonite. There is also no construction and simulation of montmorillonite molecular structure using molecular modelling method, especially the (110) edge surface since this surface often contains broken bonds which could affect its sorption ability.

1.3 Purpose

The purpose of this study is to identify the palladium-chloride species that can form in a Na-Ca-Cl saline environment using DFT simulations. The simulations can help determine the

sorption energy of each palladium-chloride species on various montmorillonite sorption sites. The study will involve calculating the free energy of the palladium-chloride species $PdCl^{+}$, $PdCl_2$, $PdCl_3^{-}$, and $PdCl_4^{2-}$. Additionally, the sorption sites of silicon and aluminum on both basal and edge surfaces of montmorillonite will be modelled. The study will also calculate the sorption energy between each palladium-chloride species and each identified sorption site. The results will then be compared to the experimental results obtained by (Nagasaki et al., 2019). If there are strong agreements between the simulation and experimental results, the result of the sorption reaction between the $PdCl_4^{2-}$ species and MX-80 bentonite being the only reaction that contribute to the sorption process can be justified.

2. Theory

2.1 Sorption Mechanisms

Sorption is a term used to describe the process by which one substance adheres to another, without specifying a particular mechanism (Hinz, 2001). Sorption encompasses both absorption and adsorption, which can occur through physical or chemical processes. Absorption involves atoms, ions, and molecules entering the bulk phase of a material (Atkins & De Paula, 2010). In solids, absorption can involve substances in both liquid and gas phases, whereas in liquids, absorption typically involves gaseous substances. Absorption is characterized by the uptake of substances into the volume of the absorbing material.

In contrast to absorption, adsorption is a surface phenomenon where atoms, ions, or molecules accumulate on the surface of a material. This process is driven by interactions between the adsorbate (the substance being adsorbed) and the adsorbent (the surface on which adsorption occurs). Adsorption can involve physical interactions, such as van der Waals forces, or chemical interactions, such as covalent or ionic bonding.

Physical adsorption, or physisorption, typically involves weaker forces and is generally reversible, allowing adsorbates to desorb when conditions change. Chemical adsorption, or chemisorption, involves stronger interactions and is often irreversible due to the formation of

strong chemical bonds. The effectiveness of adsorption depends on factors such as the surface area and porosity of the adsorbent, the nature of the adsorbate, and environmental conditions like temperature and pressure. In this study, the specific chemical sorption is focused.

The most commonly used theory to explain specific chemical sorption is called the surface complexation theory. Surface complexation occurs when ions or molecules from a solution bind to specific sites on a solid surface, forming a coordination complex. This binding can occur in two ways shown in Figure 2: inner-sphere and outer-sphere complexation. Inner-sphere complexes form when the ions or molecules make direct chemical bonds, such as covalent or ionic bonds, with the surface atoms of the solid. In this case, the ions or molecules lose their hydration shell, meaning they no longer have water molecules directly attached to them (Sposito, 1984). On the other hand, outer-sphere complexes occur when the ions or molecules retain their hydration shell and interact with the solid surface through weaker forces like electrostatic attraction or hydrogen bonding, without direct bonding to the surface atoms (Stumm, 1992). There are various surface complexation reactions explained using the surface complexation theory. The surface can go through protonation and deprotonation to form a positively charged and negatively charged surface respectively.

$$S - OH + H^+ \Leftrightarrow S - OH_2^+ \tag{2.1}$$

$$S - OH \Leftrightarrow S - O^- + H^+ \tag{2.2}$$

Metal binding and ligand exchange are shown below with an imaginary metal Me^{+z} and an imaginary ligand L^{-y} (Stumm & Morgan, 1996).

$$S - OH + Me^{+z} \Leftrightarrow S - OMe^{+(z-1)} + H^+ \tag{2.3}$$

$$S - OH + Me^{+z} + H_2O \Leftrightarrow S - OMeOH^{+(z-2)} + 2H^+ \tag{2.4}$$

$$S-OH \ + \ Me^{+z} + 2H_2O \Leftrightarrow \ S-OMe(OH)_2{}^{+(z-3)} \ + \ 3H^+ \tag{2.5}$$

$$S-OH \ + \ L^{-y} \Leftrightarrow \ S-L^{1-y} \ + \ OH^- \tag{2.6}$$

Ternary surface complex formations are also shown in equations (2.7) to (2.10).

$$S-OH \ + \ L^{-y} + Me^{+z} \Leftrightarrow \ S-OMeL^{+(z-y-1)} \ + \ H^+ \tag{2.7}$$

$$S-OH \ + \ 2L^{-y} + Me^{+z} \Leftrightarrow \ S-OMeL_2^{+(z-2y-1)} \ + \ H^+ \tag{2.8}$$

$$S-OH \ + \ 3L^{-y} + Me^{+z} \Leftrightarrow \ S-OMeL_3^{+(z-3y-1)} \ + \ H^+ \tag{2.9}$$

$$S-OH \ + \ L^{-y} + Me^{+z} + H^+ \Leftrightarrow \ S-OMeL^{+(z-y+1)} \ + \ H_2O \tag{2.10}$$

2.2 Density Functional Theory

DFT is a quantum mechanical method used to study the electronic structure of many-body systems, particularly atoms, molecules, and condensed phases. The core idea behind DFT is that the ground state properties of a many-electron system can be determined by its electron density, denoted as $\rho(\mathbf{r})$, which is a function of spatial coordinates **r** rather than its wave function, simplifying the complex problem of solving the Schrödinger equation for many electrons (Hohenberg & Kohn, 1964).

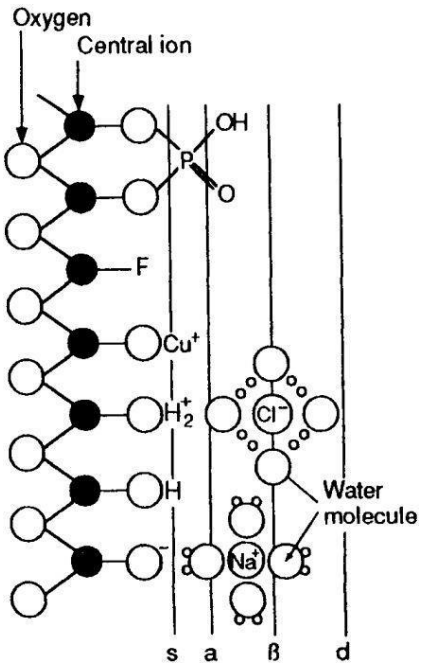

Figure 2 Examples of inner-sphere complex and outer-sphere complex. Vertical lines represent surface hydroxyl groups (s), inner-sphere complexes (a), outer-sphere complexes (b), and diffusion ion swarm (d) (Stumm, 1992).

The concept of a functional is a mapping from a space of functions to the real numbers. Unlike functions, which take numbers as inputs and produce numbers as outputs, functionals take functions as inputs. This concept is fundamental in fields like calculus of variations, quantum mechanics, and many branches of mathematical physics.

Formally, a functional F is defined as:

$$F: X \to \mathbb{R}$$

X is a space of functions. For example, if X is a space of real-valued functions defined on an interval $[a, b]$, then a functional F maps each function $f \in X$ to a real number $F(f)$.

The foundation of DFT lies in two pivotal theorems established by Hohenberg and Kohn in 1964 called the Hohenberg-Kohn Theorems. The first Hohenberg-Kohn theorem states that the ground state properties of a many-electron system are uniquely determined by its electron density, $\rho(r)$. This implies that the ground state energy and other observables can be expressed as functionals of the electron density. Mathematically, if $V(r)$ is the external potential acting on the electrons, then the total energy functional E[ρ] is uniquely determined by ρ(r):

$$E[\rho] = T[\rho] + V_{ext}[\rho] + V_{ee}[\rho] \tag{2.11}$$

In the above equation, $T[\rho]$ is the kinetic energy functional, $V_{ext}[\rho]$ is the external potential energy functional, and $V_{ee}[\rho]$ is the electron-electron interaction energy potential.

The second Hohenberg-Kohn theorem states that the correct ground state electron density minimizes the total energy functional. Therefore, the ground state energy E_0 is obtained by finding the electron density ρ_0 that minimizes $E[\rho]$:

$$E[\rho] = \min_{\rho} E[\rho] \tag{2.12}$$

To make DFT practically applicable, Kohn and Sham (1965) proposed transforming the interacting many-electron problem into a system of non-interacting electrons moving in an effective potential. This simplification retains the essential physics of electron interactions while making calculations more tractable. The Kohn-Sham equations are:

$$\left[-\frac{\hbar}{2m}\nabla^2 + v_{eff}(\mathbf{r})\right]\psi_i(\mathbf{r}) = \epsilon_i\psi_i(\mathbf{r}) \tag{2.13}$$

In the Kohn-Sham equation, $\hbar$ is the reduced Planck's constant, m is the electron mass, and ∇^2 is the Laplacian operator, which represents the kinetic energy of the electrons, $\psi_i(\mathbf{r})$ are the Kohn-Sham orbitals, and ϵ_i are their corresponding eigenvalues, which also represent energy

levels. The effective potential $v_{eff}(\mathbf{r})$ is composed of three potentials. The first potential is the external potential $v(\mathbf{r})$. This is the same potential representing electrostatic interaction between the electrons and nuclei and any other potential fields. The second potential is Hartree potential $v_H(\mathbf{r})$. This term accounts for the classical electrostatic repulsion between the electron density, and it is given by:

$$v_H(\mathbf{r}) = \int \frac{\rho(\mathbf{r}')}{|\mathbf{r} - \mathbf{r}'|} d\mathbf{r}' \tag{2.14}$$

This integral sums the electrostatic potential due to all other electrons at a point **r.** The third potential is the exchange-correlation potential $v_{xc}(\mathbf{r})$. This term includes all the complex quantum mechanical effects of electron exchange and correlation that are not captured by the Hartree potential. The exchange part arises from the Pauli exclusion principle, which requires that no two electrons can occupy the same quantum state. The correlation part accounts for the interaction among electrons due to their mutual avoidance.

The electron density $\rho(\mathbf{r})$ is derived form the Kohn-Sham orbitals as:

$$\rho(\mathbf{r}) = \sum |\psi_i(\mathbf{r})|^2 \tag{2.15}$$

The exchange-correlation functional $E_{xc}[\rho]$ is crucial for the accuracy of DFT calculations. It represents the exchange-correlation energy, encompassing the quantum mechanical exchange interactions and the dynamic correlation between electrons. Since the exact form of the exchange-correlation functional is unknown, various approximations are used with their own pros and cons.

The Local Density Approximation (LDA) assumes that the exchange-correlation energy at each point in space depends only on the electron density at that point, similar to a homogeneous electron gas. The LDA form is:

$$E_{xc}^{LDA}[\rho] = \int \rho(\mathbf{r})\epsilon_{xc}\big(\rho(\mathbf{r})\big)\, d\mathbf{r} \tag{2.16}$$

The Generalized Gradient Approximation (GGA) is an improved version of LDA by incorporating the gradient of the electron density, $\nabla\rho(\mathbf{r})$, thus accounting for the variations in electron density. The GGA form is:

$$E_{xc}^{GGA}[\rho] = \int f\big(\rho(\mathbf{r}), \nabla\rho(\mathbf{r})\big)\, d\mathbf{r} \tag{2.17}$$

Pseudopotentials are an essential concept in density functional theory (DFT) calculations, used to simplify the treatment of electron interactions, particularly in systems with heavy atoms. In quantum mechanics and DFT, solving the Schrödinger equation for many-electron systems involves significant computational challenges, especially for atoms with many electrons. The core electrons, which are close to the nucleus, contribute little to the chemical properties and bonding characteristics of atoms. Therefore, treating them explicitly in calculations is often unnecessary and computationally expensive.

Pseudopotentials address this by approximating the effects of the core electrons and the nucleus as an effective potential, allowing only the valence electrons to be explicitly treated in the calculations. This approach reduces the number of electrons that need to be considered, thus simplifying the computations (Payne et al., 1992). By eliminating the need to calculate core electron states, pseudopotentials significantly reduce the computational resources required, allowing for the study of larger systems or more complex materials within feasible timescales

(Kresse & Furthmüller, 1996). Core electrons are tightly bound to the nucleus and do not participate significantly in chemical bonding. Pseudopotentials remove the need to solve for these tightly bound states, focusing instead on the valence electrons that dictate chemical behaviour (Martin, 2004).

2.3 Basal and Edge Surfaces in Crystal Structures

In crystallography and materials science, the concepts of basal and edge surfaces are essential for understanding the properties and behaviours of crystalline materials. These surfaces are characterized using Miller indices, which are a notation system in crystallography for planes in crystal lattices. Specifically, the (001) plane often represents the basal surface, while the (110) plane can represent an edge surface.

Miller indices are a set of three integers (hkl) that describe the orientation of a plane in a crystal lattice. The indices are derived from the reciprocal of the fractional intercepts that the plane makes with the crystallographic axes. For example, the (001) plane intercepts the c-axis at one unit distance and is parallel to the a- and b-axes. The (110) plane intercepts the a- and b-axes at one unit distance and is parallel to the c-axis. These indices provide a concise way to describe the orientation and properties of different planes within a crystal, which is essential for understanding the material's overall behaviour.

The basal surface, denoted by the Miller index (001), is a plane that is parallel to the base of the crystal lattice. In hexagonal crystal systems, such as graphite and hexagonal boron nitride (h-BN), the (001) plane is perpendicular to the c-axis and parallel to the a- and b-axes. This

orientation is significant because the (001) plane is typically the most stable and energetically favourable surface within the crystal structure.

The Miller index (001) indicates that the plane intercepts the c-axis at one unit distance and is parallel to both the a- and b-axes. This is a basal plane because it lies parallel to the crystallographic axes a and b, forming a flat, stable surface. For example, in graphite, the basal planes (001) consist of layers of carbon atoms arranged in a hexagonal lattice. These layers are held together by weak van der Waals forces, allowing them to slide over each other easily, which contributes to graphite's lubricating properties (Zhao & Xue, 2020).

The edge surface, often represented by the Miller index (110), is a plane that is perpendicular to the basal plane and parallel to the edges of the crystal. The (110) plane is less stable and more reactive compared to the basal (001) plane due to the higher density of unsatisfied bonds or "dangling bonds." These surfaces are important in materials like graphite and h-BN because they significantly influence the material's reactivity and interaction with other substances.

The Miller index (110) indicates that the plane intercepts the a- and b-axes at one unit distance and is parallel to the c-axis. This plane is an edge surface because it intersects the crystal edges and is perpendicular to the basal plane. In layered materials, the edge surfaces (110) are critical for defining how the material interacts with its environment and how it can be chemically modified. For instance, during the exfoliation of graphite to produce graphene, the properties of the edge surfaces influence the ease of layer separation and the resultant quality of the graphene sheets (Santos et al., 2016).

3. Sorption Simulation Methods

3.1 Benchmark

A benchmark paper was used to justify the methodology of calculating sorption energies between palladium-chloride species and montmorillonite surfaces using DFT calculations. If a paper investigated sorption mechanisms between a target fission product in used nuclear fuel and a solid surface using DFT, benchmark simulations could help replicating the results from the paper. If the replication process was successful, the target fission product would be substituted with palladium-chloride species and the solid surface would be substituted with montmorillonite surfaces using DFT. The results obtained should make sense because the same process and calculations were used in the benchmark paper.

Sample benchmark simulations are conducted based on the works from (Puhakka et al., 2019), where the sorption energies between Se(IV) species and the edge surfaces of phlogopite were calculated using the CASTEP (CAmbridge Serial Total Energy Package) (Clark et al., 2005) algorithm in the Materials Studio software.

Table 1 Sorption energies of Se(IV) species onto phlogopite edge surface (Puhakka et al., 2019)

Se species	Phlogopite (110) (eV)
$Se(IV)O_3^{2-}$	6.4
$HSe(IV)O_3^-$	4.5
$H_2Se(IV)O_4$	0.7

The sorption energies are calculated using the equation below:

$$E_{sorption} = E_{Absorbent} + E_{solvent} - E_{solution} \quad (3.1)$$

The positivity of the sorption energies shown in Table 1 elucidates that the sorption of $Se(IV)O_3^{2-}$, $HSe(IV)O_3^-$, and $H_2Se(IV)O_4$ will not happen on the phlogopite edge surface because the reactions will be endothermic due to having more energies in the final state than the initial state.

If the results could be replicated by using the same setup in Materials Studio, then by replacing the Se(IV) species with Pd species and the phlogopite edge surface with montmorillonite basal and edge surfaces, the sorption mechanism between Pd and montmorillonite in a saline environment can be investigated and justified. Based on this methodology, sample benchmark simulations are done to try to replicate the same results. The model of phlogopite is from the default module in Materials Studio. Sorption model of $Se(IV)O_3^{2-}$, $HSe(IV)O_3^-$, and $H_2Se(IV)O_4$ onto phlogopite edge surface is constructed as shown in Figure 3 to 5.

The unit cell of the molecular structure of montmorillonite was constructed with a lattice parameter of a = 2023 pm, b = 534 pm, and c = 1976 pm. The total thickness of the surface model was 1.011 nm. A vacuum slab perpendicular to the surface was 1.0 nm. All the above parameters used is identical from (Puhakka et al., 2019). The exchange-correlation was implemented with generalized gradient approximation GGA-PBE, which is a functional within DFT that offers a good balance between accuracy and computational cost. The purpose of the benchmark is not to obtain exact numbers, but rather to achieve similar numbers that lead to the same conclusions. To prioritize computational time over the accuracy of calculations, the norm conserving pseudopotentials are used for all elements of phlogopite and Se(IV) species. The potentials used were H_00PBE_OP.recpot for hydrogen, O_00PBE_OP.recpot for oxygen, Mg_00PBE_OP.usp for magnesium, Al_00.recpot for aluminum, Si_00PBE_OP.recpot for silicon, and K_00.recpot for potassium. These are ultrasoft pseudopotentials used for their efficiency in large systems. The kinetic cut-off energy for the plane-wave expansion of the wave function was 500 eV for the sorption models, also used from (Puhakka et al., 2019).

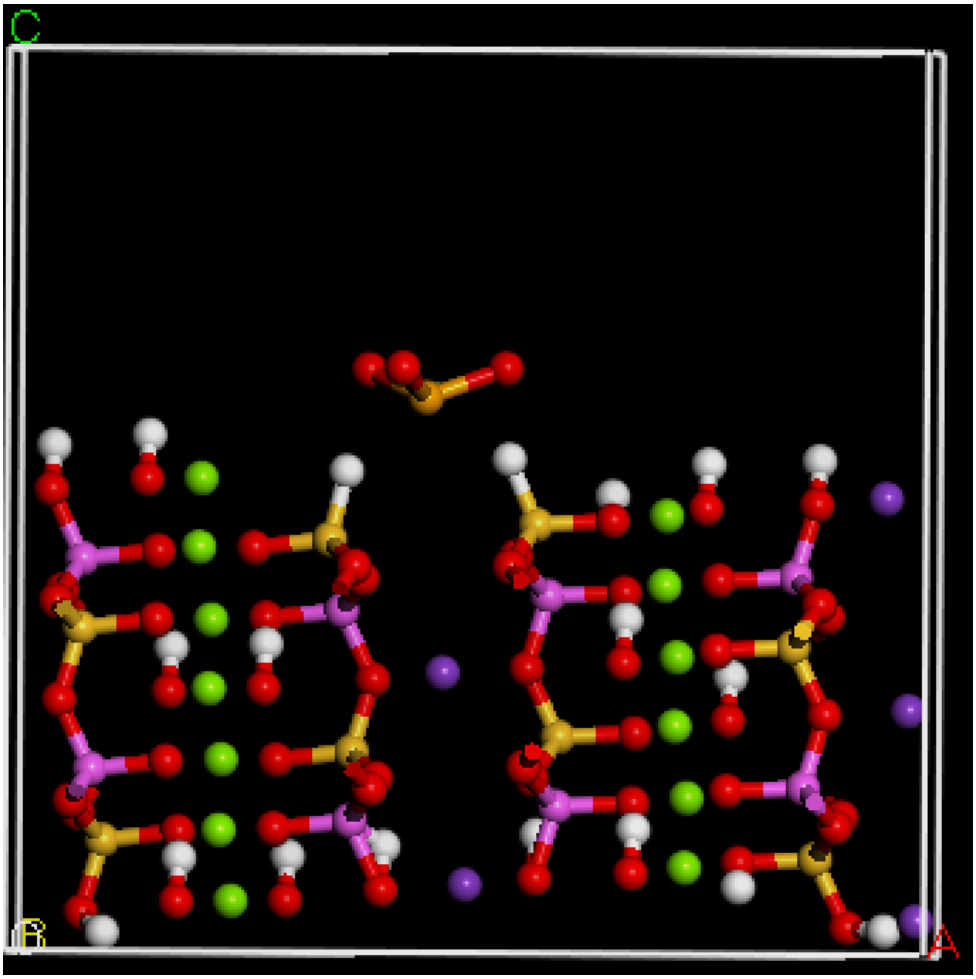

Figure 3 Sorption model of $Se(IV)O_3^{2-}$ onto phlogopite (110) surface. H – white, O – red, Si – yellow, Mg – green, Al – pink, K - purple

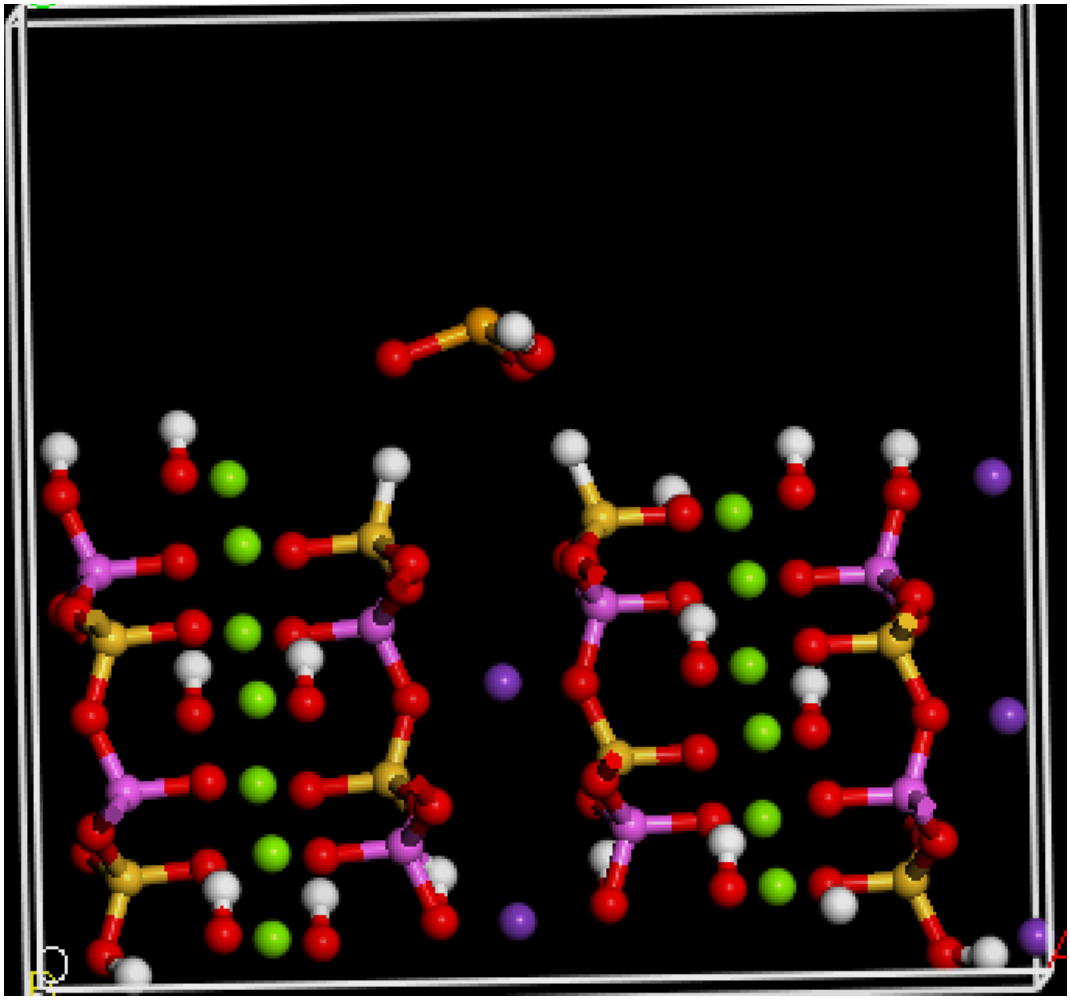

Figure 4 Sorption model of $HSe(IV)O_3^-$ onto phlogopite (110) surface. H – white, O – red, Si – yellow, Mg – green, Al – pink, K - purple

A)

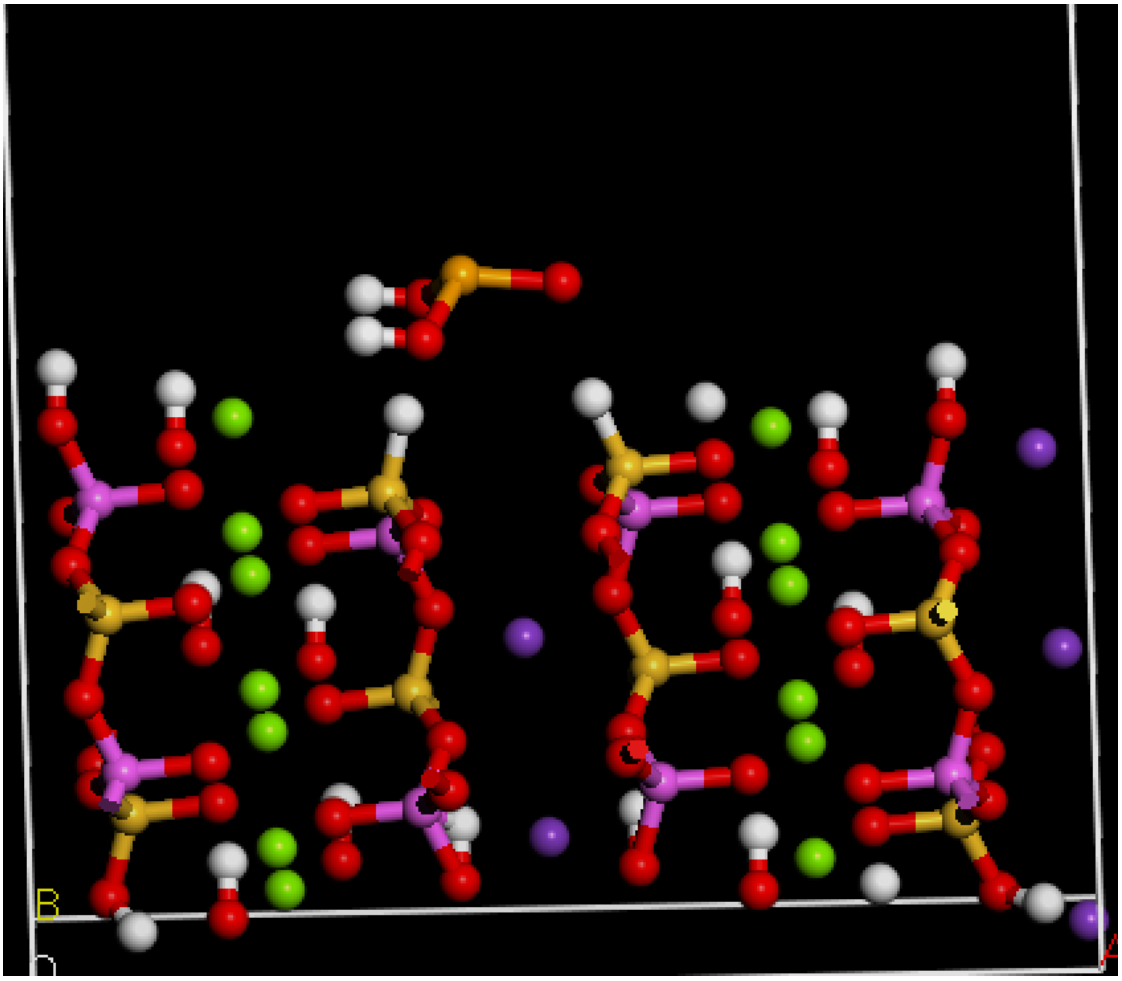

Figure 5 Sorption model of $H_2Se(IV)O_4$ onto phlogopite (110) surface. H – white, O – red, Si – yellow, Mg – green, Al – pink, K - purple

3.2 Palladium-chloride Models

In the literature review, it was found out that palladium cations could form various palladium-chloride complexes in a saline environment where the chloride anions are rich in

presence. To further investigate which kind of palladium-chloride complexes could form, the molecular geometry of $PdCl^+$, $PdCl_2$, $PdCl_3^-$, and $PdCl_4^{2-}$ are optimized by DFT calculations in Materials Studio. Fifty water molecules are also manually added into the models to simulate the water environment as shown in Figure 6. The black space in the figure represents vacuum. However, palladium-chloride species are forming in aqueous environment in the DGR. Adding water molecules would simulate the real-life scenario. There is no significant reason for selecting the number fifty for water molecules. The module provided by the software to add water molecules in batches can only add 10 per batch, and 50 water molecules are just enough to fill up the volume of a default unit cell. The Free energies of the species are calculated using the CASTEP algorithm.

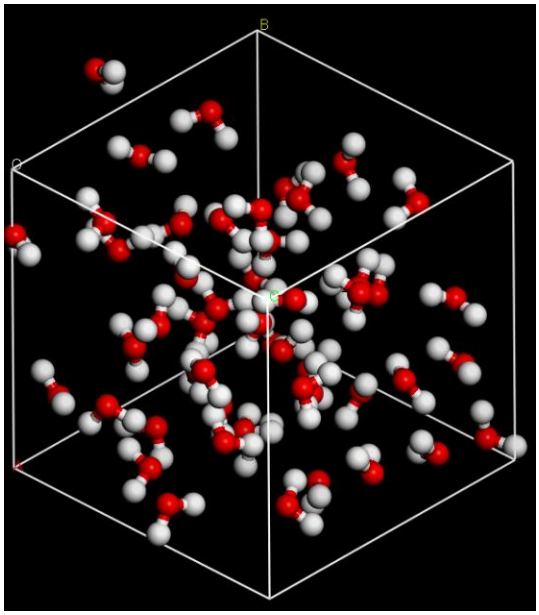

Figure 6 Total number of 50 water molecules in one unit cell

3.3 Pd Sorption onto Montmorillonite

The sorbent material investigated in this study was montmorillonite, the key component of bentonite clay. The theoretical chemical formula of montmorillonite is $(OH)_4Si_8Al_4Mg_4O_{20}\cdot nH_2O$ (Zoveidavianpoor, 2018). It is structured in layers, featuring a sheet-like arrangement. This material is distinguished by its characteristic expandable lattice, which is a result of the water molecules intercalating between the negatively charged layers of silicate. The bonding between these layers is relatively weak, which is why it can expand and contract based on the water content as shown in Figure 7. Water molecules were manually added in between layers of montmorillonite unit cell model to imitate the real-life scenario of the bentonite clay material absorbing the underground water.

The sorption reactions investigated for silicon sorption sites are:

$$\mathrm{Si-OH} + \mathrm{PdCl^+} \Leftrightarrow \mathrm{Si-OPdCl} + \mathrm{H^+} \tag{3.2}$$

$$\mathrm{Si-OH} + \mathrm{PdCl_2} \Leftrightarrow \mathrm{Si-OPdCl_2^-} + \mathrm{H^+} \tag{3.3}$$

$$\mathrm{Si-OH} + \mathrm{PdCl_3^-} \Leftrightarrow \mathrm{Si-OPdCl_3^{2-}} + \mathrm{H^+} \tag{3.4}$$

$$\mathrm{Si-OH} + \mathrm{PdCl_4^{2-}} \Leftrightarrow \mathrm{Si-OPdCl_4^{3-}} + \mathrm{H^+} \tag{3.5}$$

The sorption reactions investigated for aluminum sorption sites are:

$$\mathrm{Al-OH} + \mathrm{PdCl^+} \Leftrightarrow \mathrm{Al-OPdCl} + \mathrm{H^+} \tag{3.6}$$

$$\mathrm{Al-OH} + \mathrm{PdCl_2} \Leftrightarrow \mathrm{Al-OPdCl_2^-} + \mathrm{H^+} \tag{3.7}$$

$$Al - OH + PdCl_3^- \Leftrightarrow Al - OPdCl_3^{2-} + H^+ \quad (3.8)$$

$$Al - OH + PdCl_4^{2-} \Leftrightarrow Al - OPdCl_4^{3-} + H^+ \quad (3.9)$$

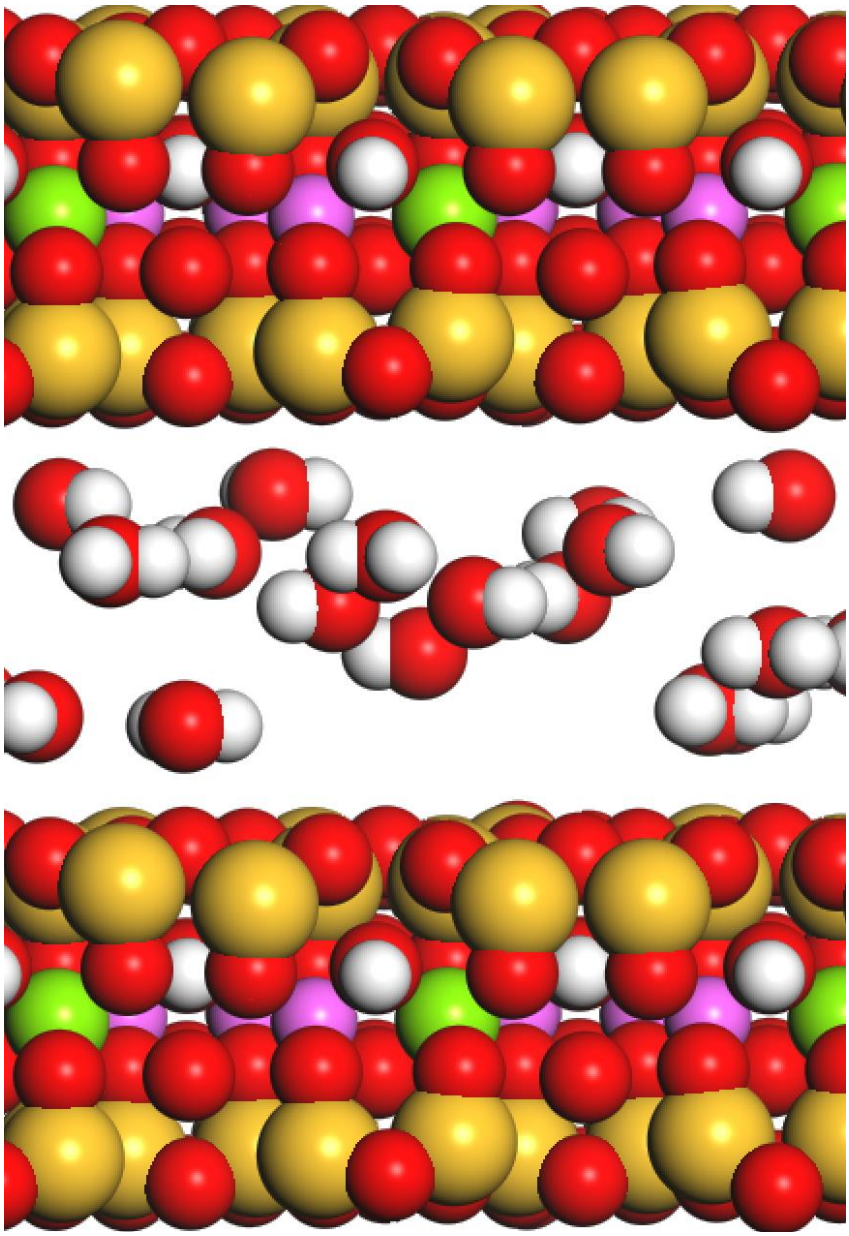

Figure 7 The layered structure of montmorillonite with water molecules between layers; H – white, O – red, Si – yellow, Mg – green, Al – pink

Both the edge (110) and basal (001) surfaces of montmorillonite with silicon and aluminium sorption sites, and the (001) surface with magnesium sorption site were examined. The modelling involves constructing three-dimensional atomistic models and calculating the total electronic energy and the overall electronic density distribution to define stable-energy structures for minerals and sorbing species (Leach, 2001). In saline Na-Ca-Cl solutions, the palladium aqueous chemistry will be mainly driven by complexation against soft ligands such as chloride (Colàs et al., 2021, 2022). In this study, the palladium-chloride species including $PdCl^+$, $PdCl_2$, $PdCl_3^-$, and $PdCl_4^{2-}$ were considered as sorbing species. The formation of palladium-chloride species in the saline Na-Ca-Cl conditions has been taken care of in the previous section. The unit cell of the molecular structure of montmorillonite was constructed with a lattice parameter of a = 1036 pm, b = 3596 pm, and c = 1840 pm. The total thickness of the surface model was 2.054 nm. A vacuum slab perpendicular to the surface was 1.0 nm.

The exchange-correlation was implemented with generalized gradient approximation GGA-PBE. To balance between the computational time and accuracy of calculations, the ultrasoft pseudopotentials were used for all elements in montmorillonite and palladium-chloride species. The potentials used were H_00PBE.usp for hydrogen, O_00PBE.usp for oxygen, Mg_00PW91.usp for magnesium, Al_00PBE.usp, Si_00PBE.usp for silicon, Cl_00PBE.usp for chloride, and Pd_00PBE.usp for palladium. The kinetic cut-off energy for the plane-wave expansion of the wave function was 380 eV for montmorillonite models. The cut-off energy was adjusted for faster convergence time before each calculation.

4. Results and Analysis

4.1 Benchmark

Table 2 shows the benchmark simulation results of the sorption energies of Se(IV) species onto phlogopite edge surface.

Table 2 Benchmark sorption energies of Se(IV) onto phlogopite edge surface

Se species	Phlogopite (110) (Benchmark) (eV)	Phlogopite (110) (Puhakka et al., 2019) (eV)
$Se(IV)O_3^{2-}$	5.3	6.4
$HSe(IV)O_3^-$	2.7	4.5
$H_2Se(IV)O_4$	1.4	0.7

The benchmark results show the same positivity from the sorption energies of $Se(IV)O_3^{2-}$, $HSe(IV)O_3^-$, and $H_2Se(IV)O_4$, which also indicate that sorption will not happen on the phlogopite edge surface due to the reactions requiring more energy to reach the final states from the initial states. Since the benchmark results reach agreement with the original study from Puhakka et al. (2019), the methodology of substituting Se(IV) species with Pd species and phlogopite edge surfaces with the basal and edge surfaces of montmorillonite can be properly justified, the

sorption mechanism between Pd and montmorillonite in a saline environment can be investigated.

4.2 Palladium-chloride Species Models

The free energies of a palladium ion, a chloride ion, and a water molecule used for the initial state total energy are modelled and calculated by DFT shown in Table 3.

Table 3 Free energies of Pd^{2+}, Cl^-, and H_2O calculated by DFT

Particles	Free energy (eV)
Pd^{2+}	-800.27
Cl^-	-413.46
H_2O	-473.69

The free energies of four palladium-chloride species $PdCl^+$, $PdCl_2$, $PdCl_3^-$, and $PdCl_4^{2-}$ surrounded by 50 water molecules used for the final state total energy are modelled and calculated by DFT shown in Table 4.

Table 4 Free energies of $PdCl^+$, $PdCl_2$, $PdCl_3^-$, and $PdCl_4^{2-}$ with 50 water molecules calculated by DFT

$PdCl_x$	Free energy (eV)
$PdCl^+$	-24902.05

$PdCl_2$	-25316.89
$PdCl_3^-$	-25729.51
$PdCl_4^{2-}$	-26142.86

Table 5 Difference between final state and initial state free energies of Pd-Cl species

$PdCl_x$	**Free energy (eV)**
$PdCl^+$	-3.82
$PdCl_2$	-5.20
$PdCl_3^-$	-4.36
$PdCl_4^{2-}$	-4.25

The existence of $PdCl^+$, $PdCl_2$, $PdCl_3^-$, and $PdCl_4^{2-}$ complexes in the Na-Ca-Cl saline environment is supported by the calculated negative free energy. The molecular geometry is optimized as well shown in Figure 8.

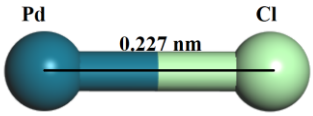

A)

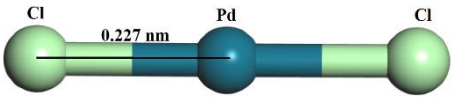

B)

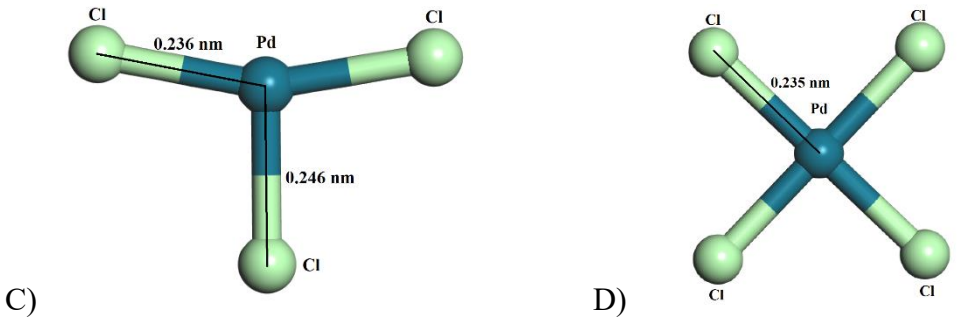

Figure 8 Molecular geometry of (A) $PdCl^+$, (B) $PdCl_2$, (C) $PdCl_3^-$, and (D) $PdCl_4^{2-}$

4.3 Pd sorption onto Montmorillonite

The free energies of one unit cell of montmorillonite silicon and aluminum sorption site on the basal (001) and edge (110) surface with water molecules for the initial state total energy are calculated by DFT. Silicon and aluminum sorption sites on the basal (001) and edge (110) surfaces of montmorillonite are shown in Figure 9 to 12. Calculation results are shown in Table 6. The sorption of $PdCl^+$, $PdCl_2$, $PdCl_3^-$, and $PdCl_4^{2-}$ on each type of sorption site on montmorillonite are shown in Figure 13 to 28.

Table 6 Free energies of Montmorillonite sorption sites with water molecules

Sorption site	Free energy (eV)
(001) Si	-163476.49
(001) Al	-155391.79
(110) Si	-170241.42
(110) Al	-167221.11

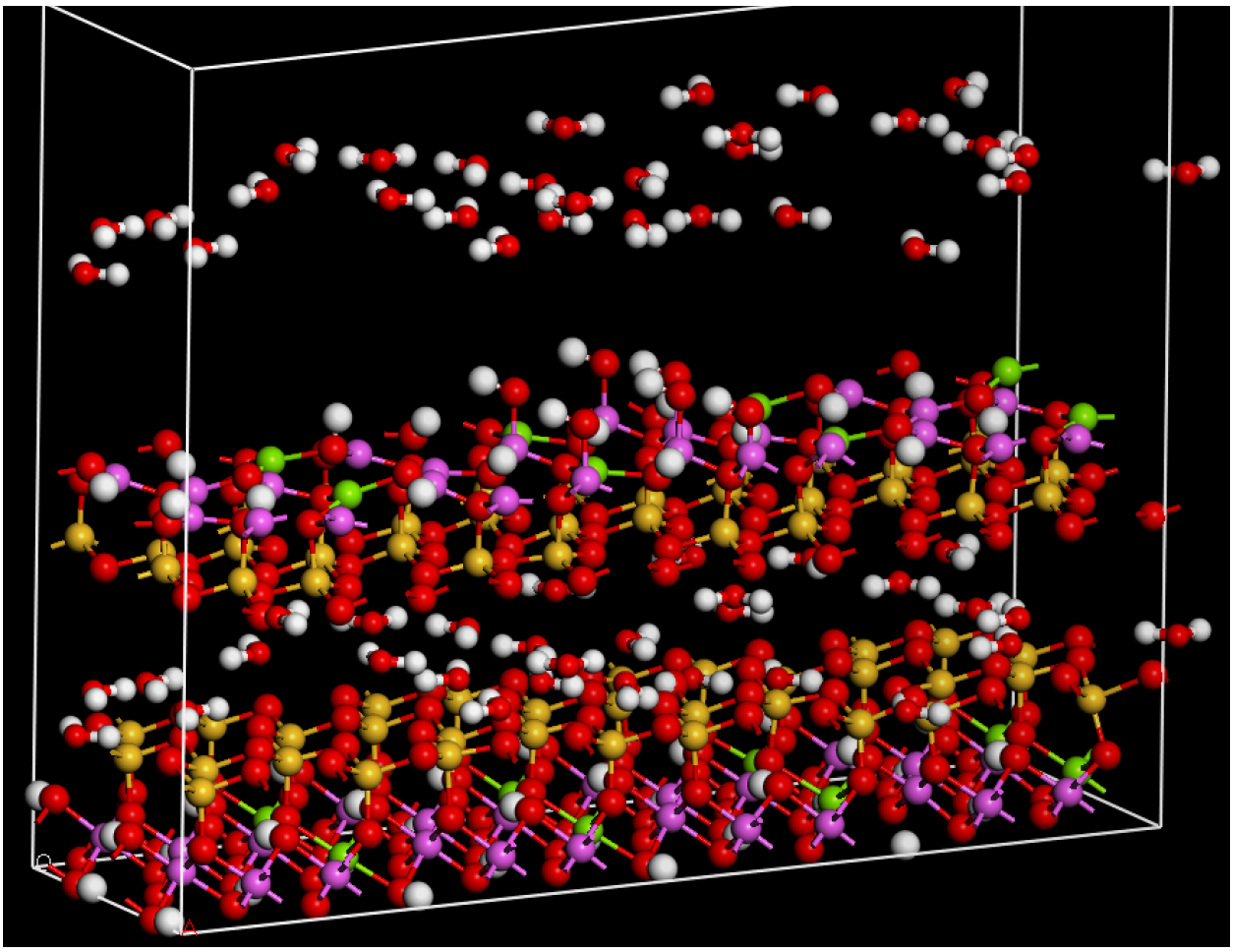

Figure 9 Al sorption site on the basal (001) surface of a unit cell of Montmorillonite

The free energies of $PdCl^{+}$, $PdCl_2$, $PdCl_3^{-}$, and $PdCl_4^{2-}$ for the initial state are calculated by DFT shown in Table 7.

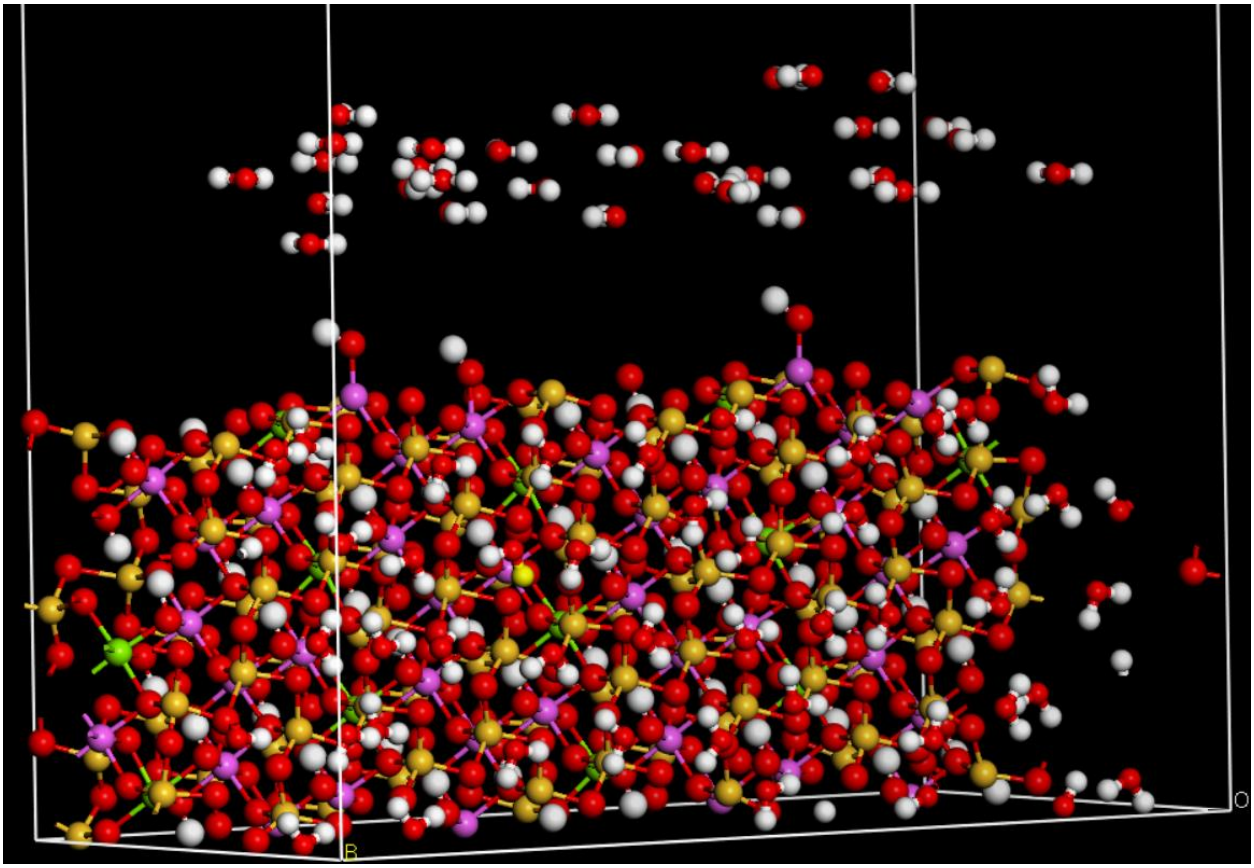

Figure 10 Al sorption site on the edge (110) surface of a unit cell of Montmorillonite

Table 7 Free energies of Pd-Cl species without water

$PdCl_x$	Free energy (eV)
$PdCl^+$	-1211.19
$PdCl_2$	-1632.39
$PdCl_3^-$	-2045.01
$PdCl_4^{2-}$	-2458.36

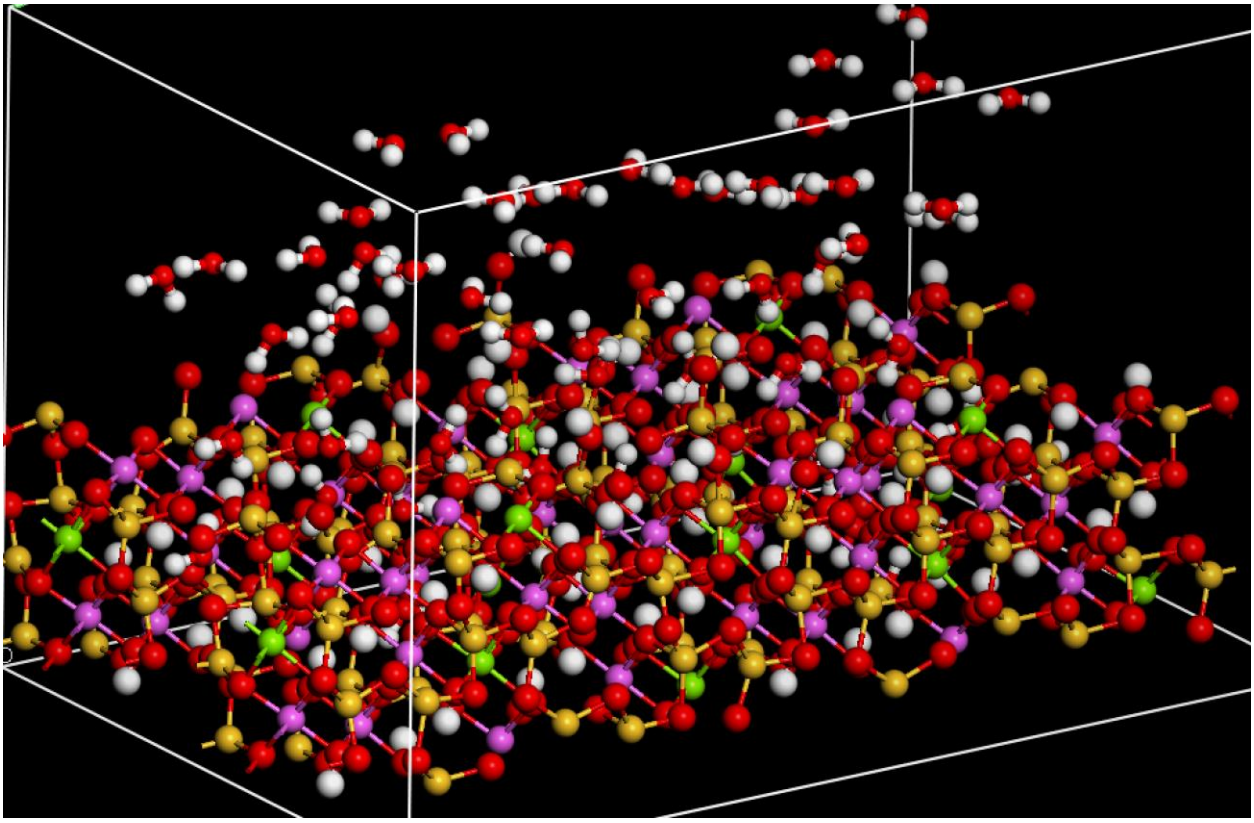

Figure 11 Si sorption site on the edge (110) surface of a unit cell of Montmorillonite

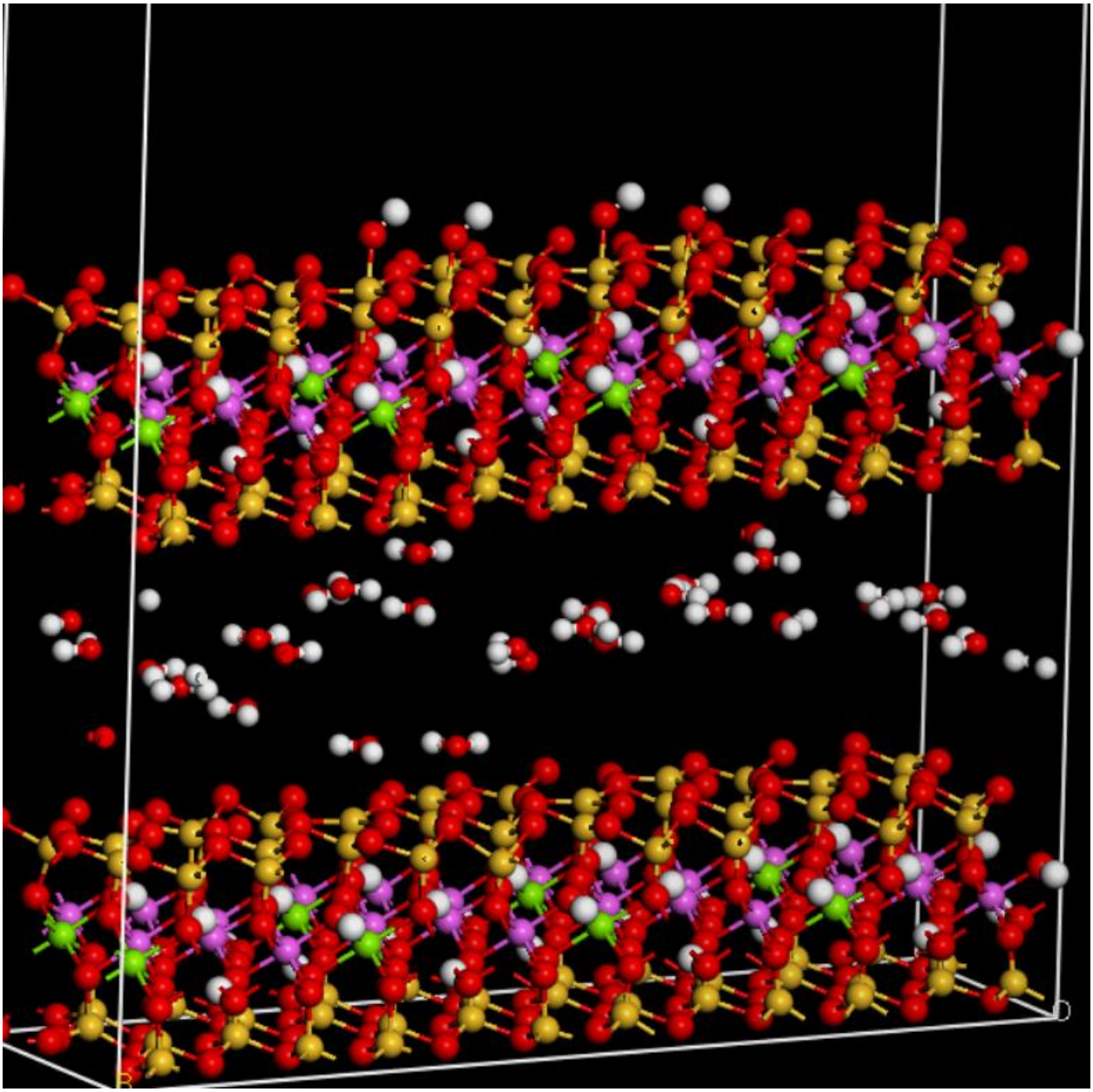

Figure 12 Si sorption site on the basal (001) surface of a unit cell of Montmorillonite

The free energies of final states of palladium-chloride species onto montmorillonite basal and edge surface sorption sites with water are calculated by DFT shown in Table 8. The free energy of a single hydrogen cation for final state calculations is -17.81 eV calculated by DFT.

Table 8 free energies of final states of palladium-chloride species onto montmorillonite basal and edge surface sorption sites

$PdCl_x$ Species	**Montmorillonite surfaces**			
	Si sorption site		Al sorption site	
	(001)	(110)	(001)	(110)
$PdCl^+$	-164670.37	-171435.90	-156586.07	-168415.89
$PdCl_2$	-165091.87	-171857.30	-157009.07	-168838.59
$PdCl_3^-$	-165504.79	-172271.02	-157423.39	-169252.81
$PdCl_4^{2-}$	-165925.74	-172687.27	-157842.94	-169668.96

By subtracting the total free energy of the initial state from the total free energy of the final state, the sorption energy of all four palladium-chloride species onto montmorillonite basal and edge surface Si and Al sorption site is calculated and shown in Table 9.

Table 9 Sorption energies (eV) of the PdCl species onto montmorillonite surfaces

$PdCl_x$ Species	**Montmorillonite surfaces**			
	Silicon sorption site		Aluminium sorption site	
	(001)	(110)	(001)	(110)
$PdCl^+$	-0.5	-1.1	-0.9	-1.4
$PdCl_2$	-0.8	-1.3	-2.7	-2.9
$PdCl_3^-$	-1.1	-2.4	-4.4	-4.5
$PdCl_4^{2-}$	-8.7	-5.3	-10.6	-7.3

The exothermic sorption energies for the Pd species on montmorillonite show that the surface complexation reactions can take place on both the basal (001) and edge (110) surfaces with both silicon and aluminium sorption sites. By comparing the absolute value of the sorption energies, it was found that the sorption energy decreases in the order of $PdCl^+$ < $PdCl_2$ < $PdCl_3^-$ < $PdCl_4^{2-}$. This is in alignment with the works by Nagasaki et al. (2019). Therefore, the most favourable palladium chloride species in the sorption reactions onto montmorillonite in the saline environment is $PdCl_4^{2-}$, followed by $PdCl_3^-$, $PdCl_2$ and $PdCl^+$.

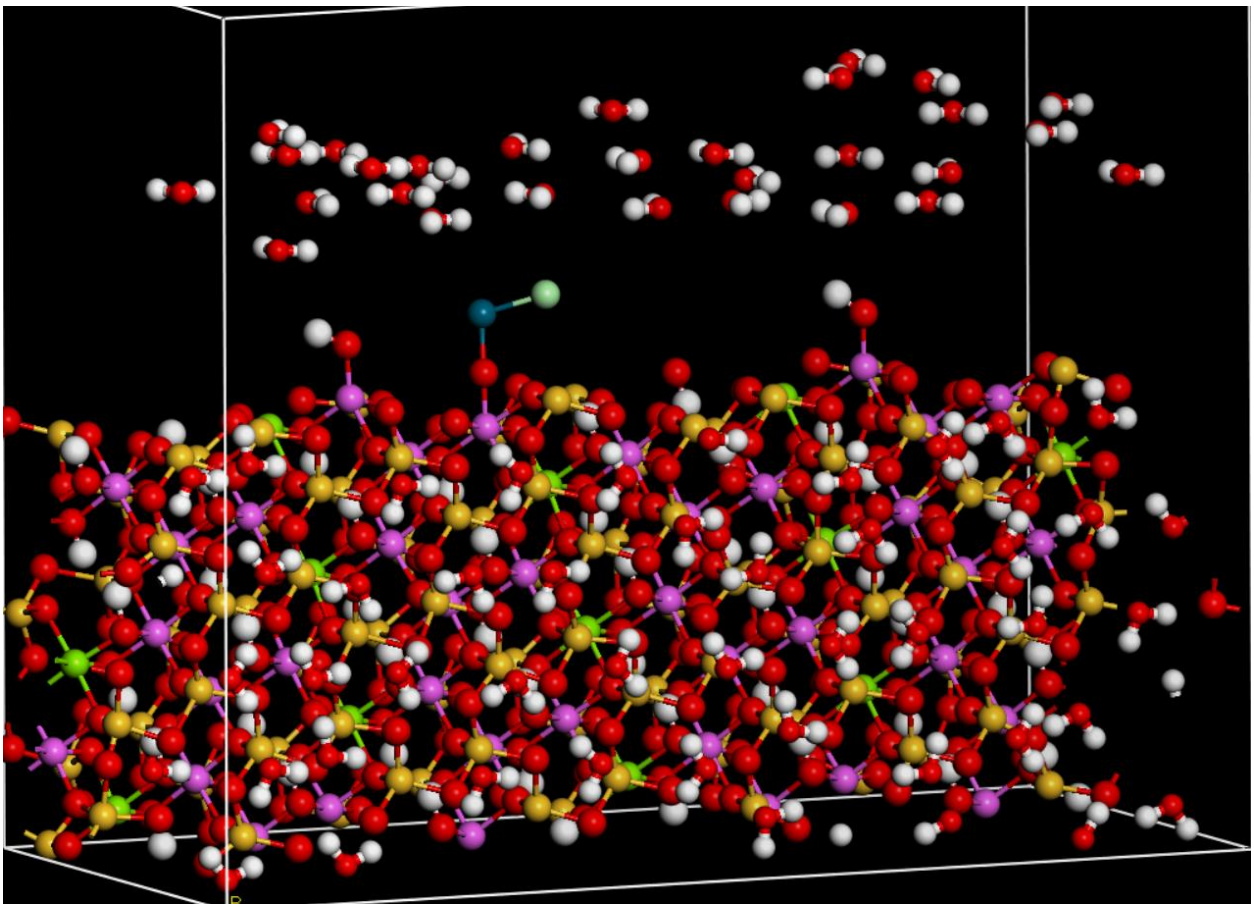

Figure 13 Sorption of $PdCl^+$ on the Al sorption site of (110) montmorillonite surface

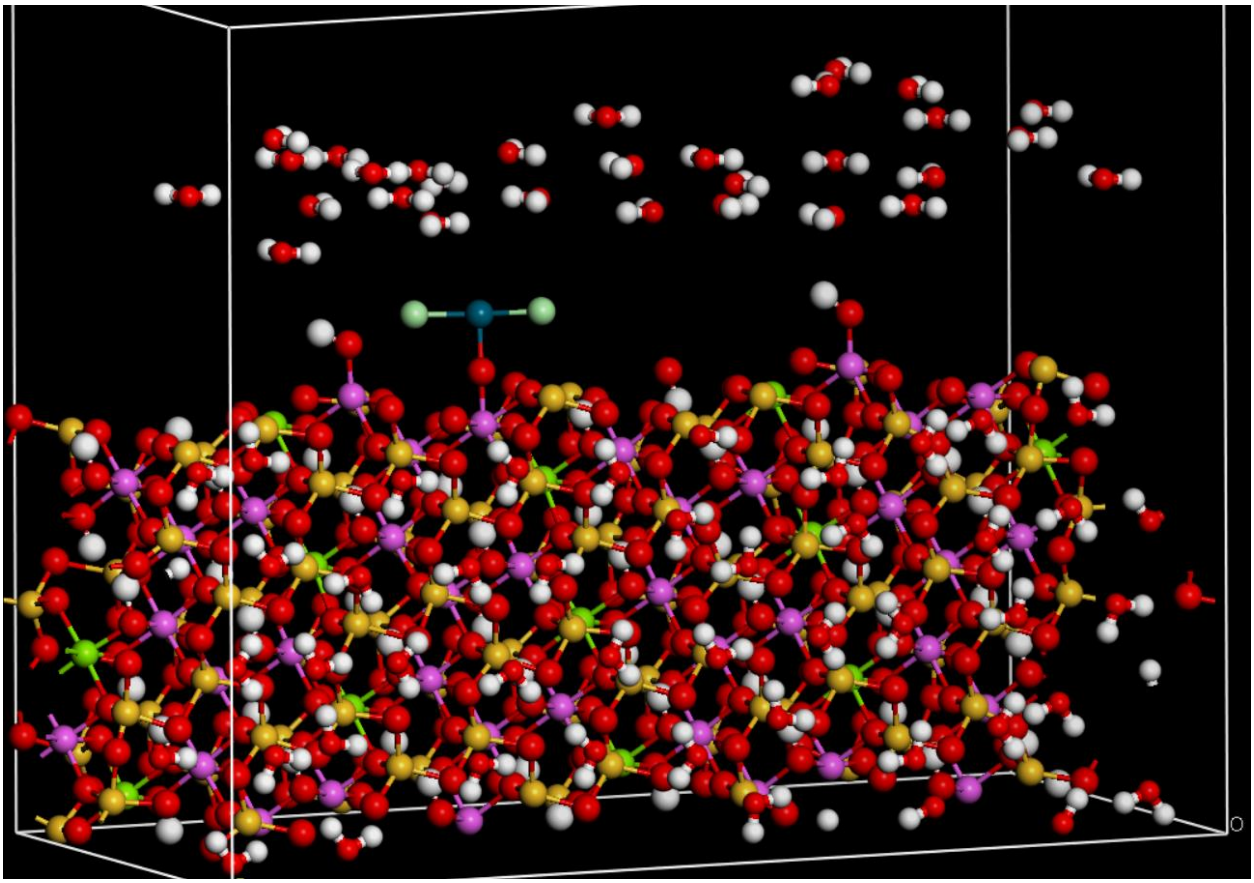

Figure 14 Sorption of $PdCl_2$ on the Al sorption site of (110) montmorillonite surface

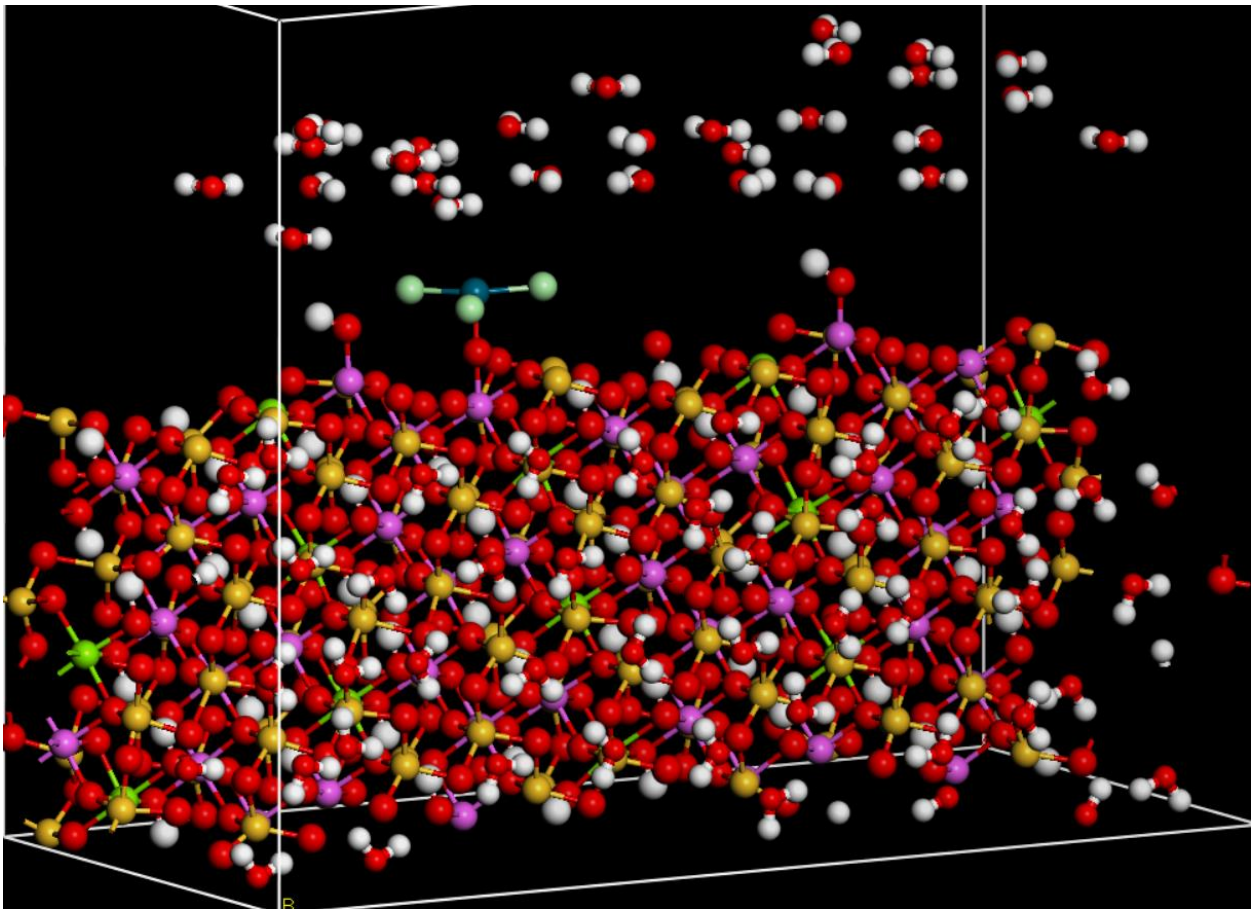

Figure 15 Sorption of $PdCl_3^-$ on the Al sorption site of (110) montmorillonite surface

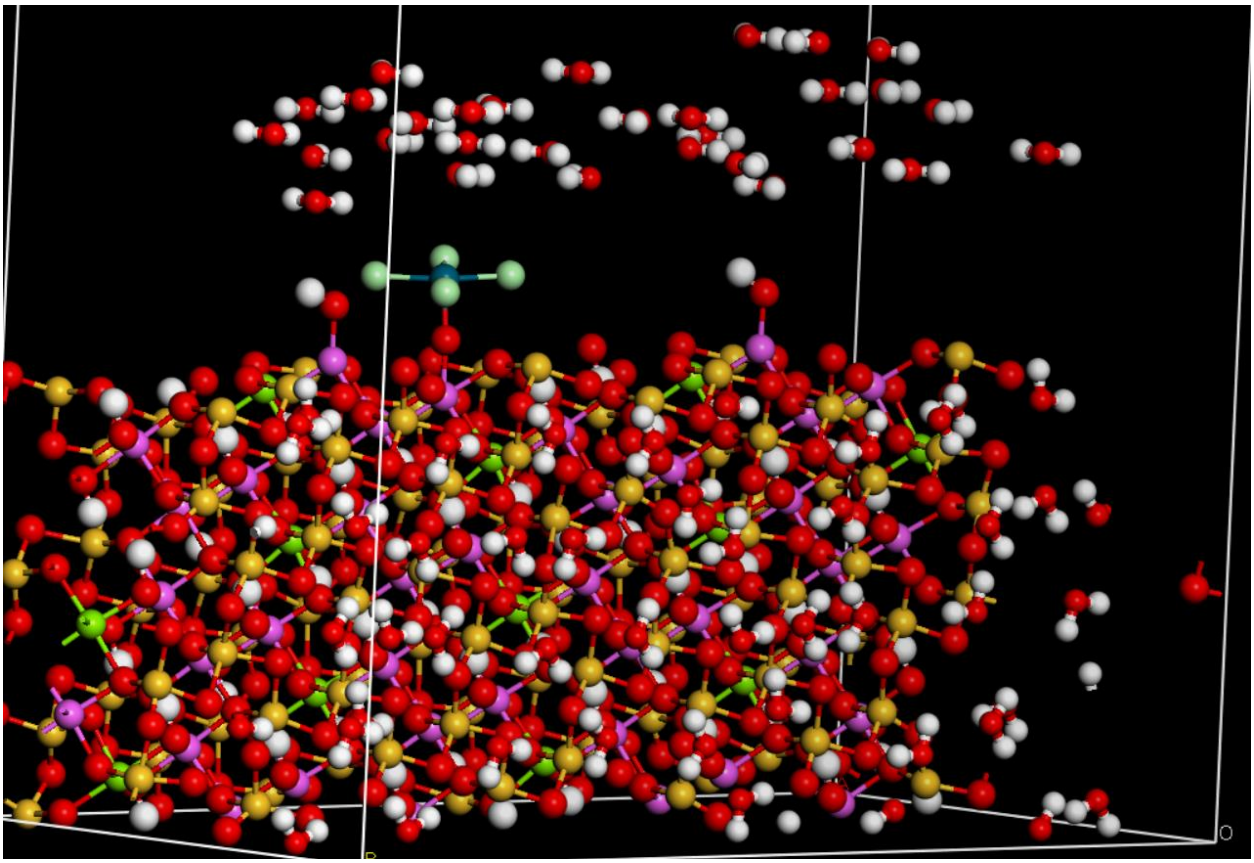

Figure 16 Sorption of $PdCl_4^{2-}$ on the Al sorption site of (110) montmorillonite surface

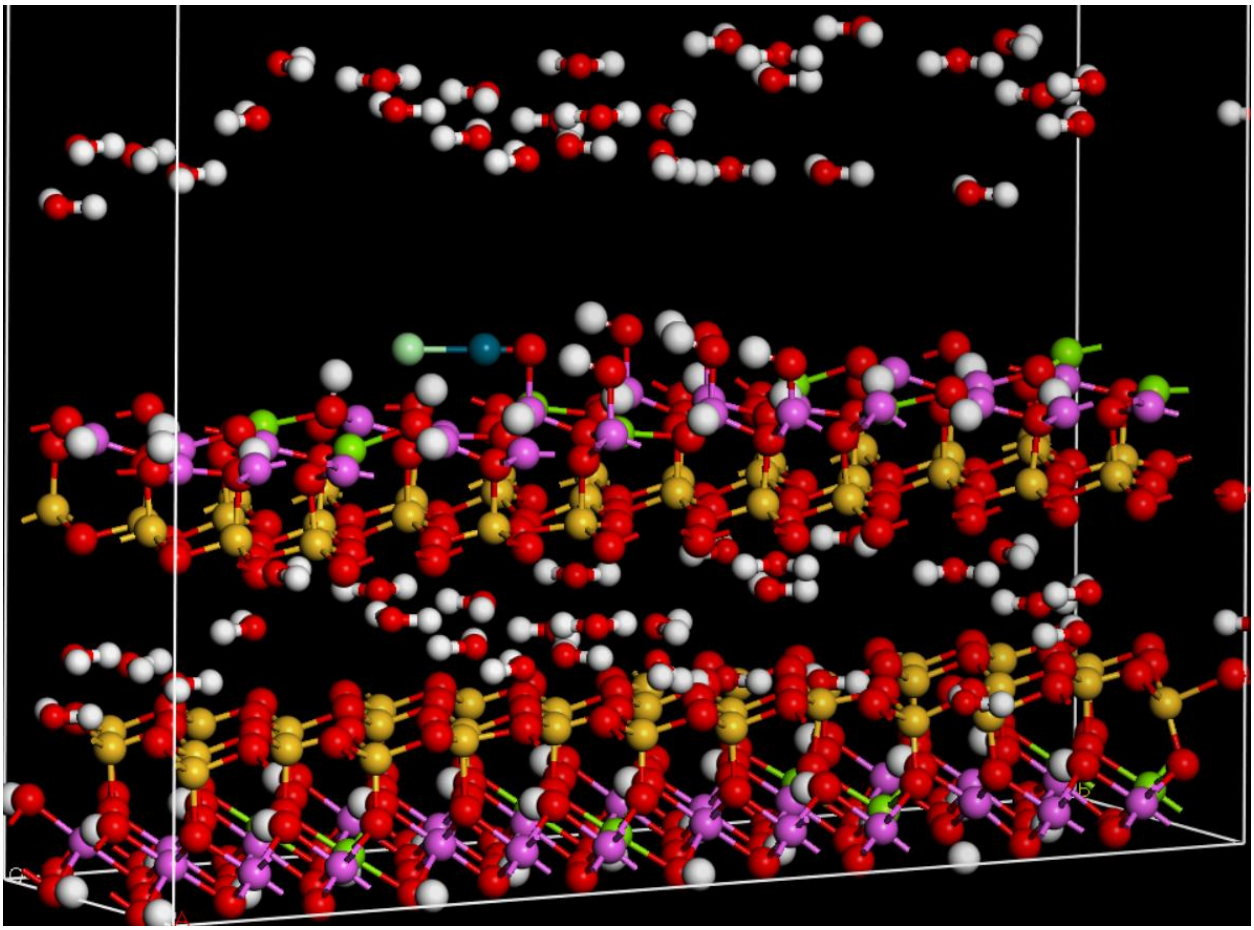

Figure 17 Sorption of $PdCl^+$ on the Al sorption site of (001) montmorillonite surface

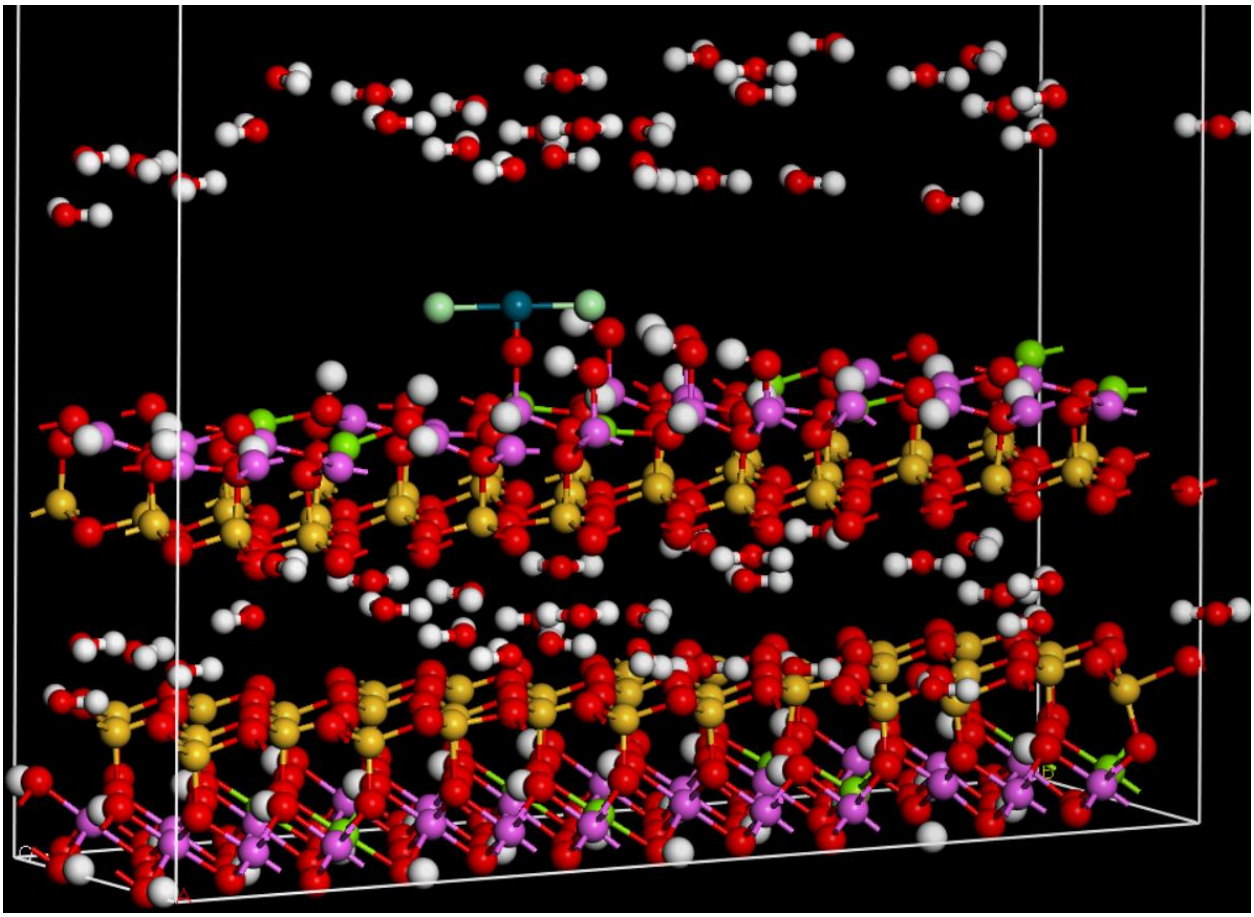

Figure 18 Sorption of $PdCl_2$ on the Al sorption site of (001) montmorillonite surface

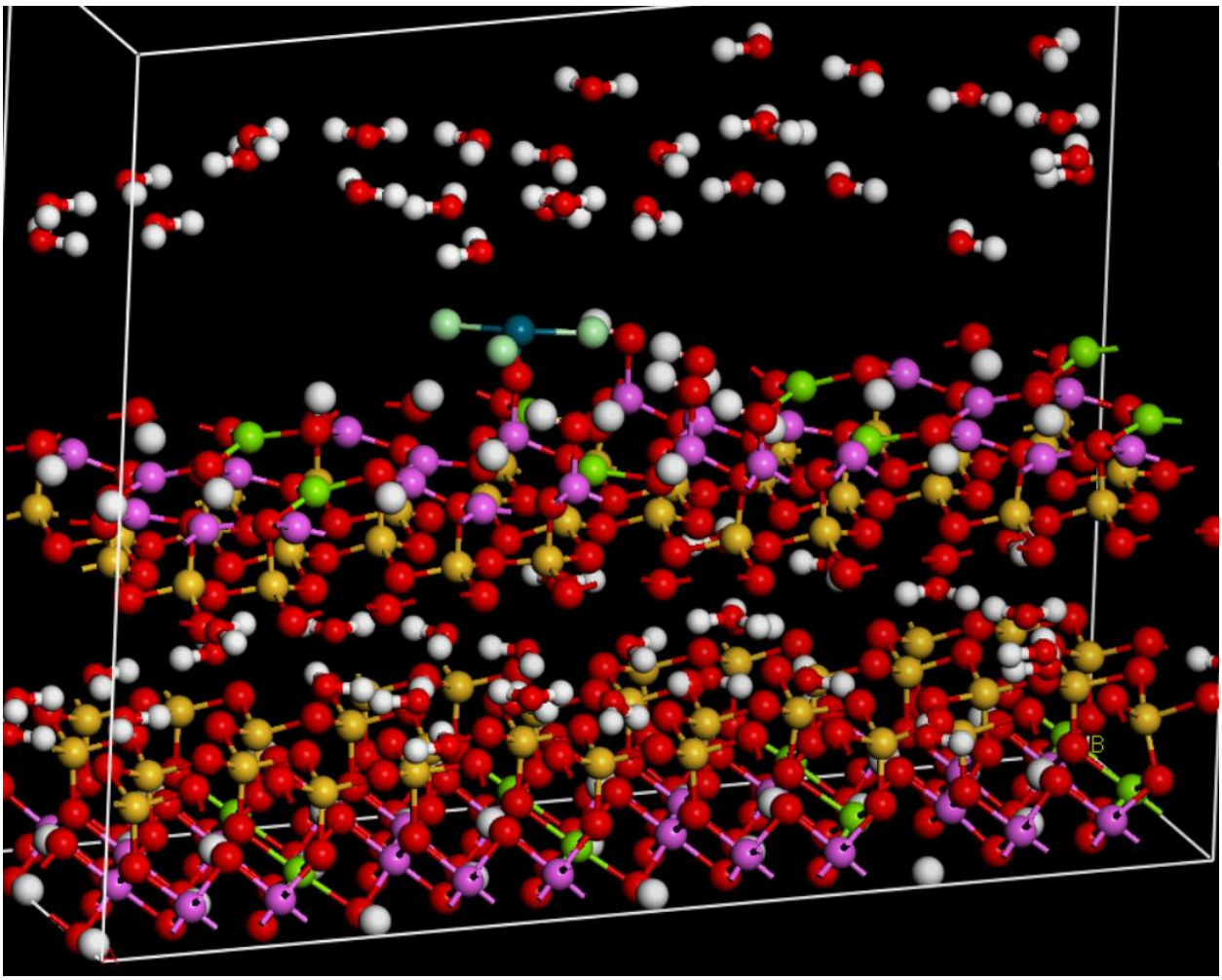

Figure 19 Sorption of $PdCl_3^-$ on the Al sorption site of (001) montmorillonite surface

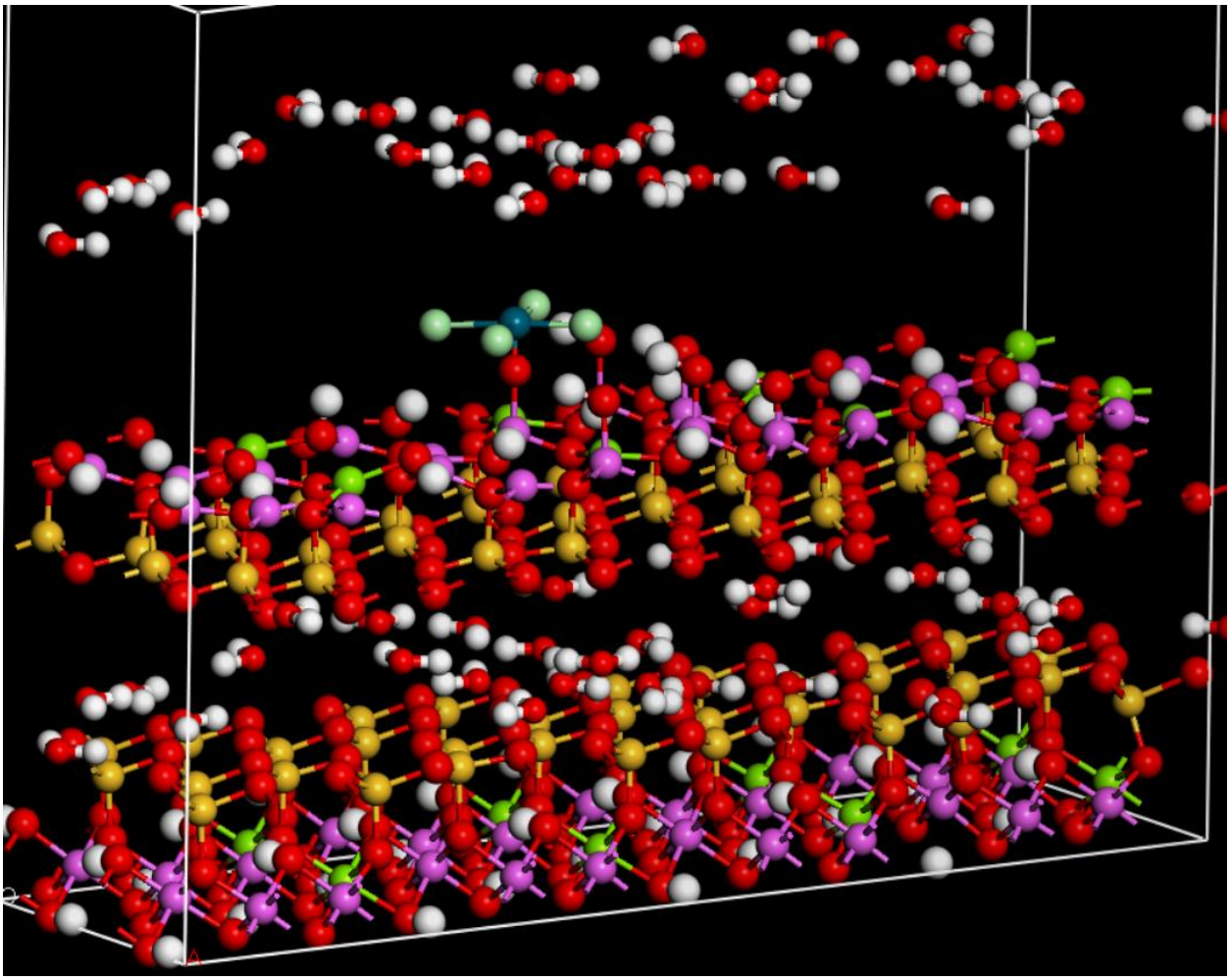

Figure 20 Sorption of $PdCl_4^{2-}$ on the Al sorption site of (001) montmorillonite surface

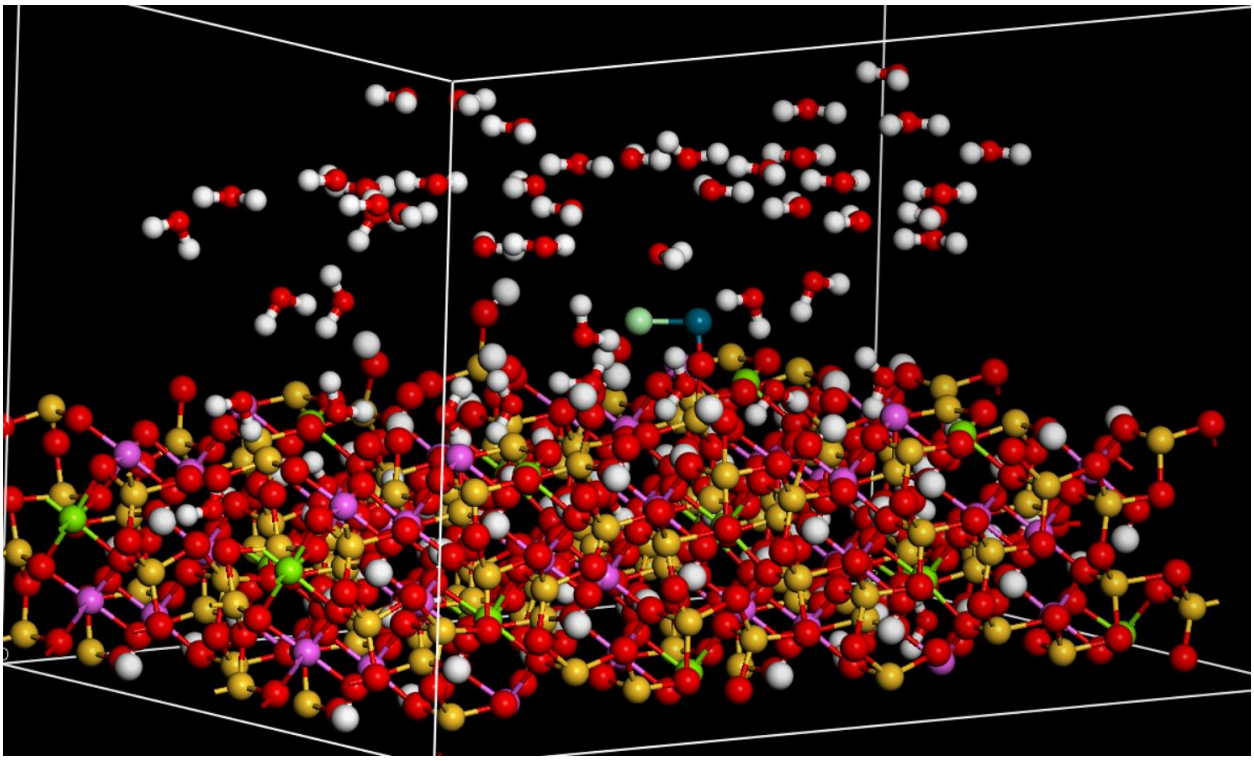

Figure 21 Sorption of $PdCl^-$ on the Si sorption site of (110) montmorillonite surface

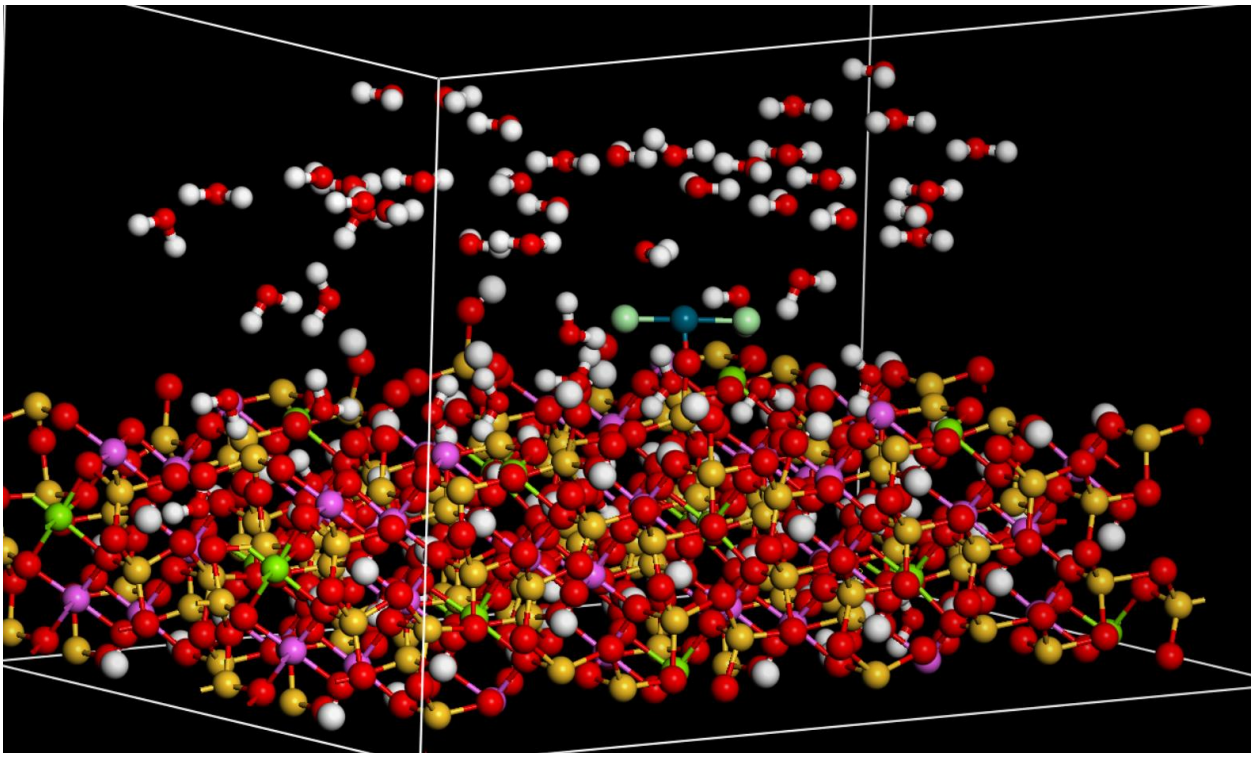

Figure 22 Sorption of $PdCl_2$ on the Si sorption site of (110) montmorillonite surface

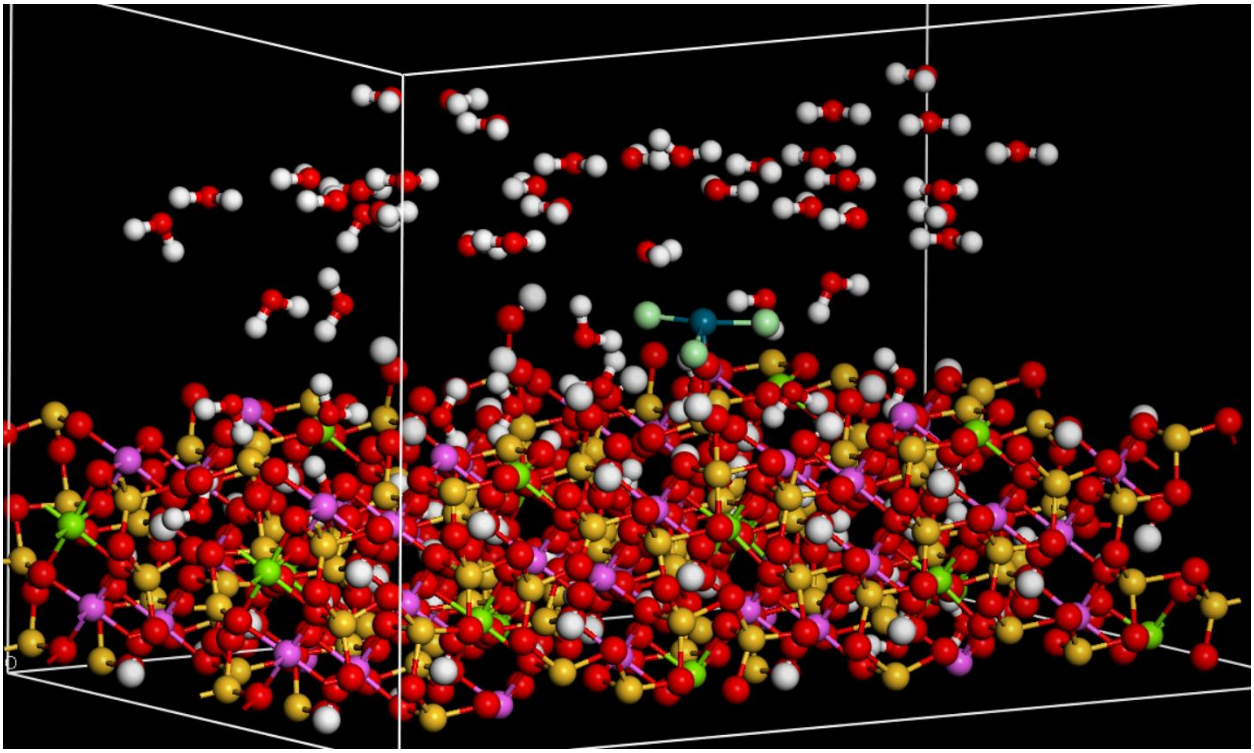

Figure 23 Sorption of $PdCl_3^-$ on the Si sorption site of (110) montmorillonite surface

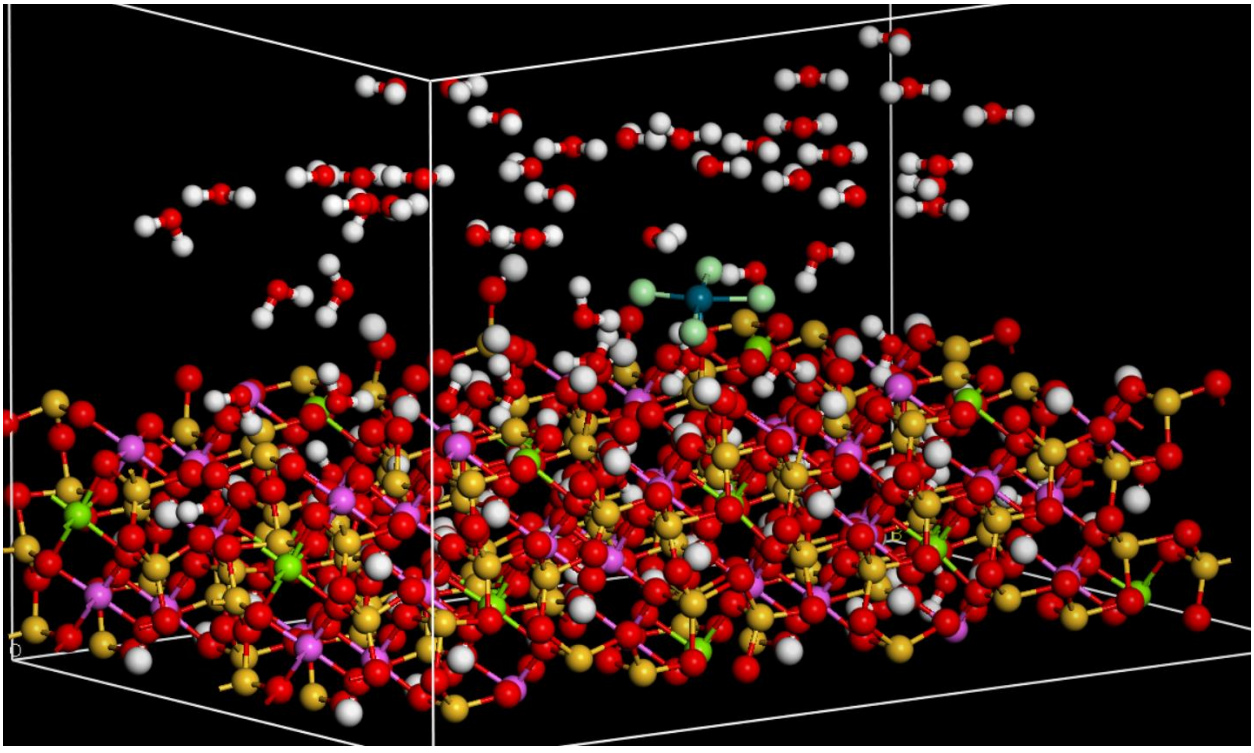

Figure 24 Sorption of $PdCl_4^{2-}$ on the Si sorption site of (110) montmorillonite surface

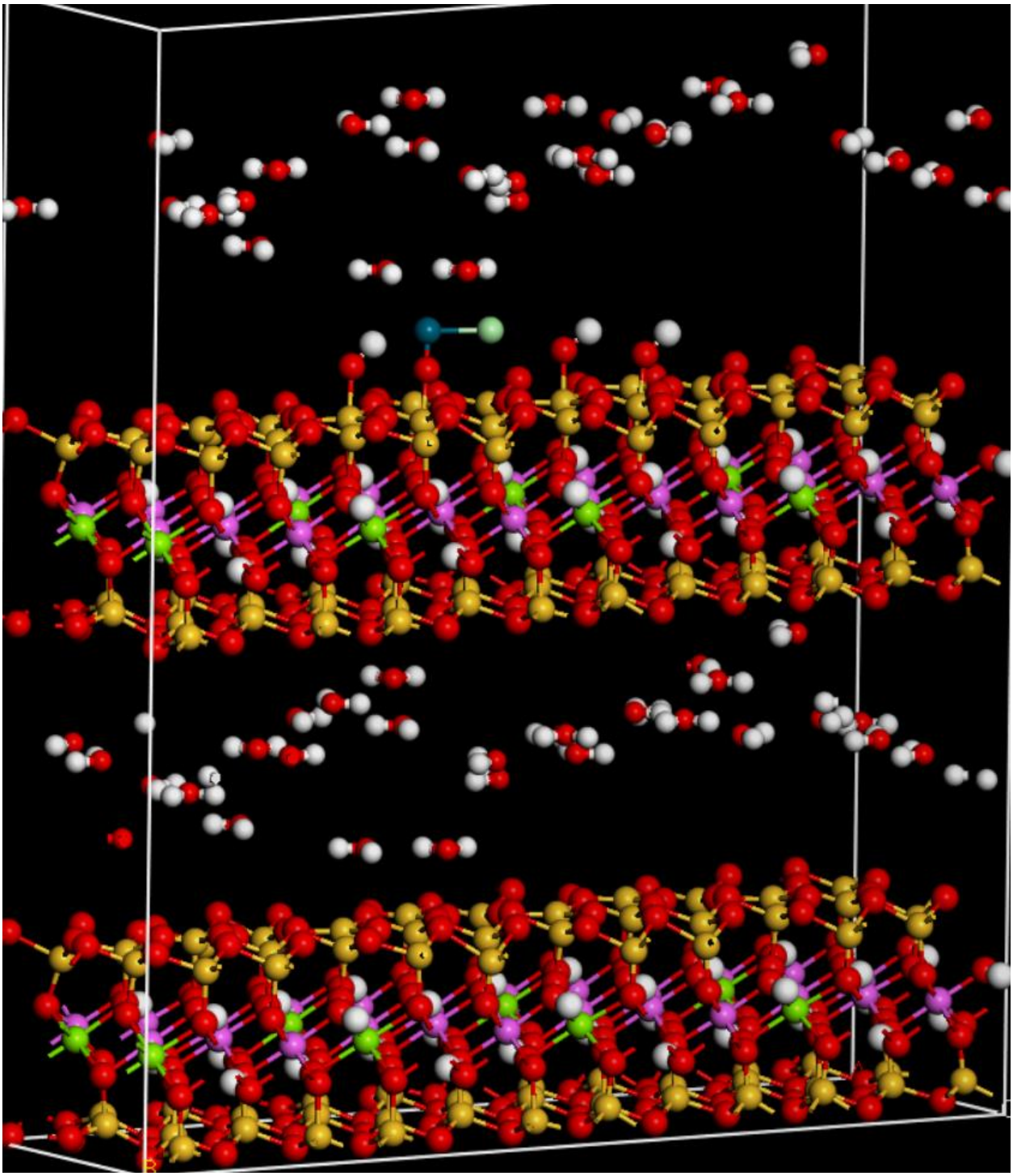

Figure 25 Sorption of $PdCl^+$ on the Si sorption site of (001) montmorillonite surface

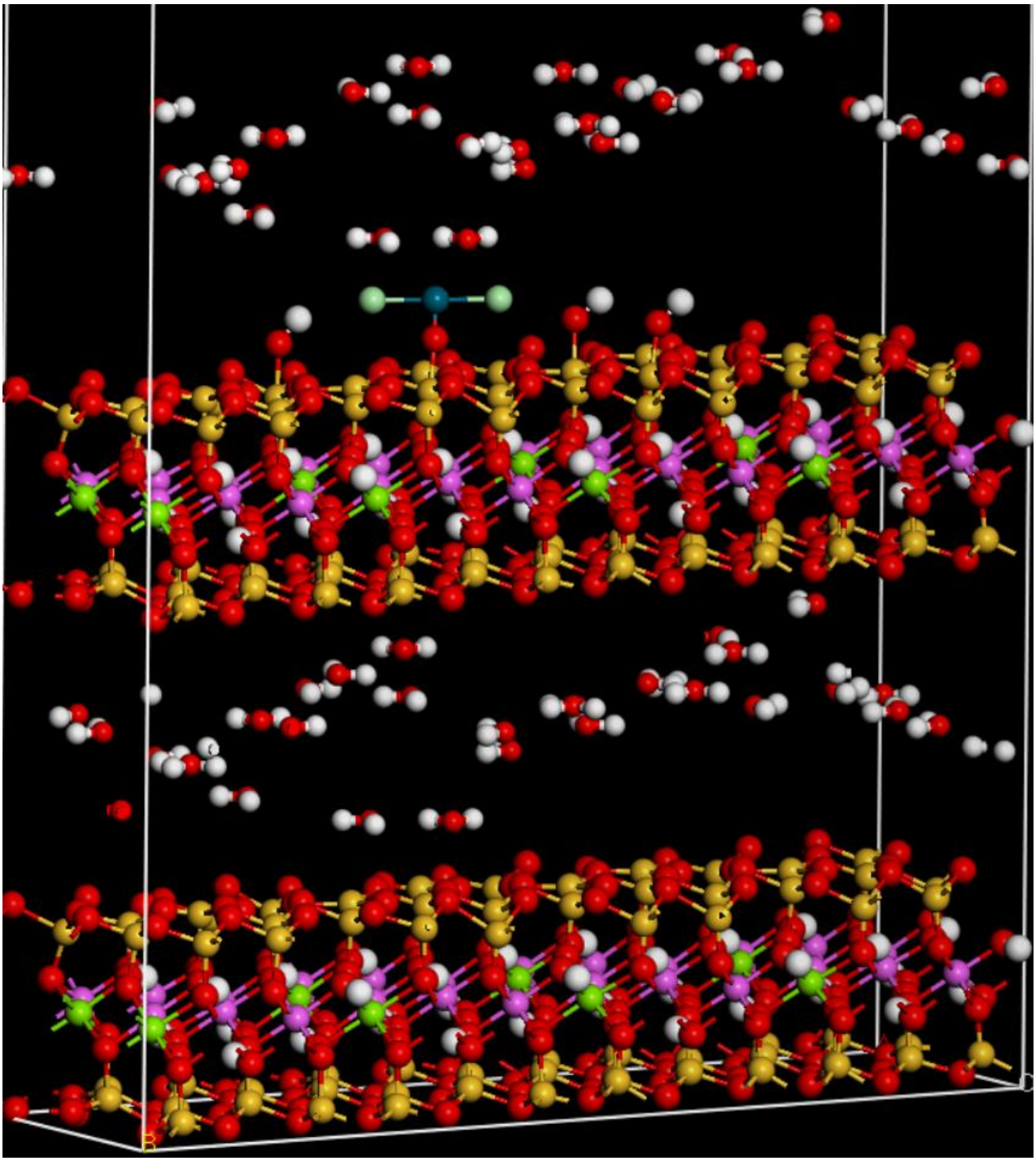

Figure 26 Sorption of $PdCl_2$ on the Si sorption site of (001) montmorillonite surface

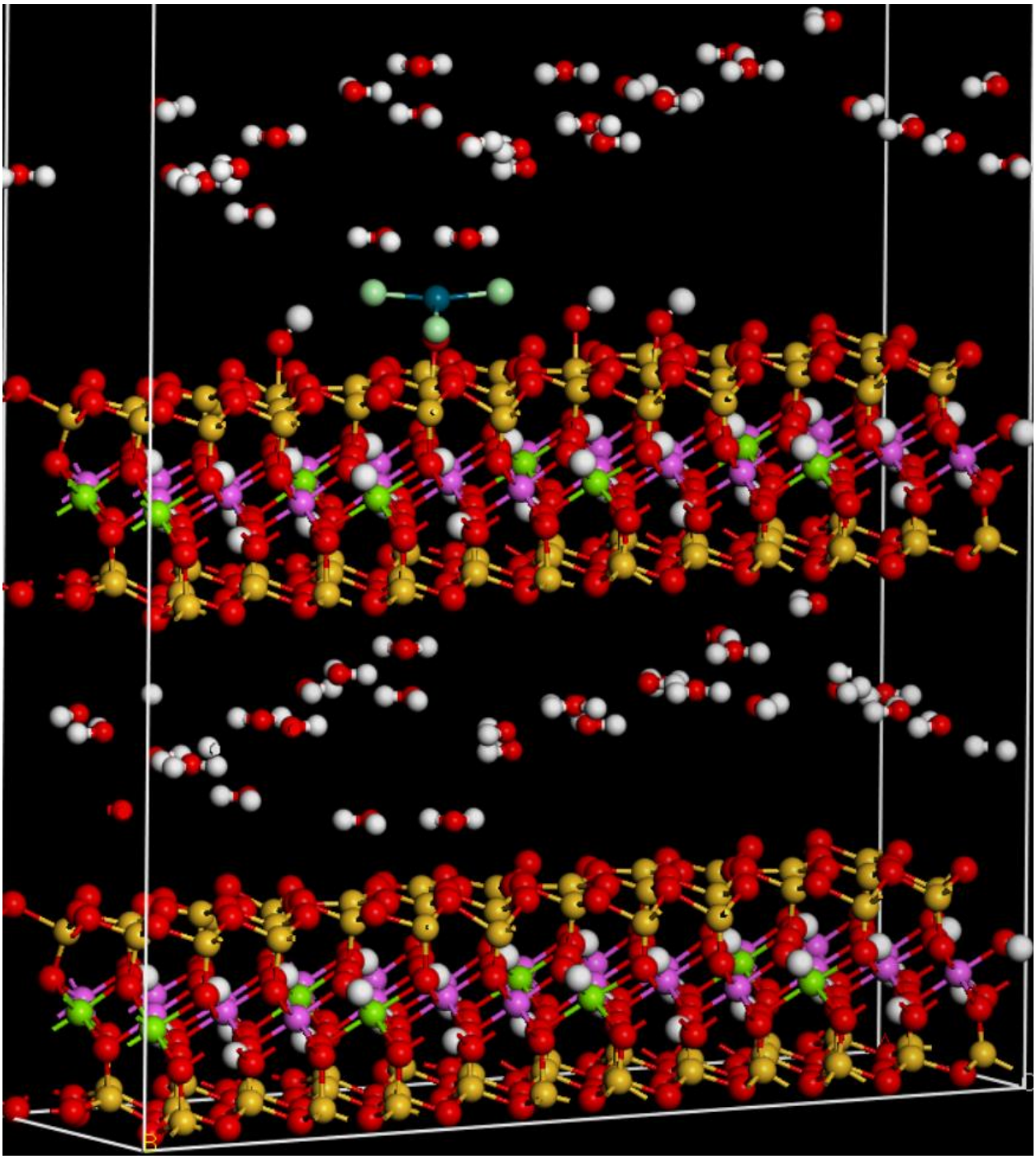

Figure 27 Sorption of $PdCl_3^-$ on the Si sorption site of (001) montmorillonite surface

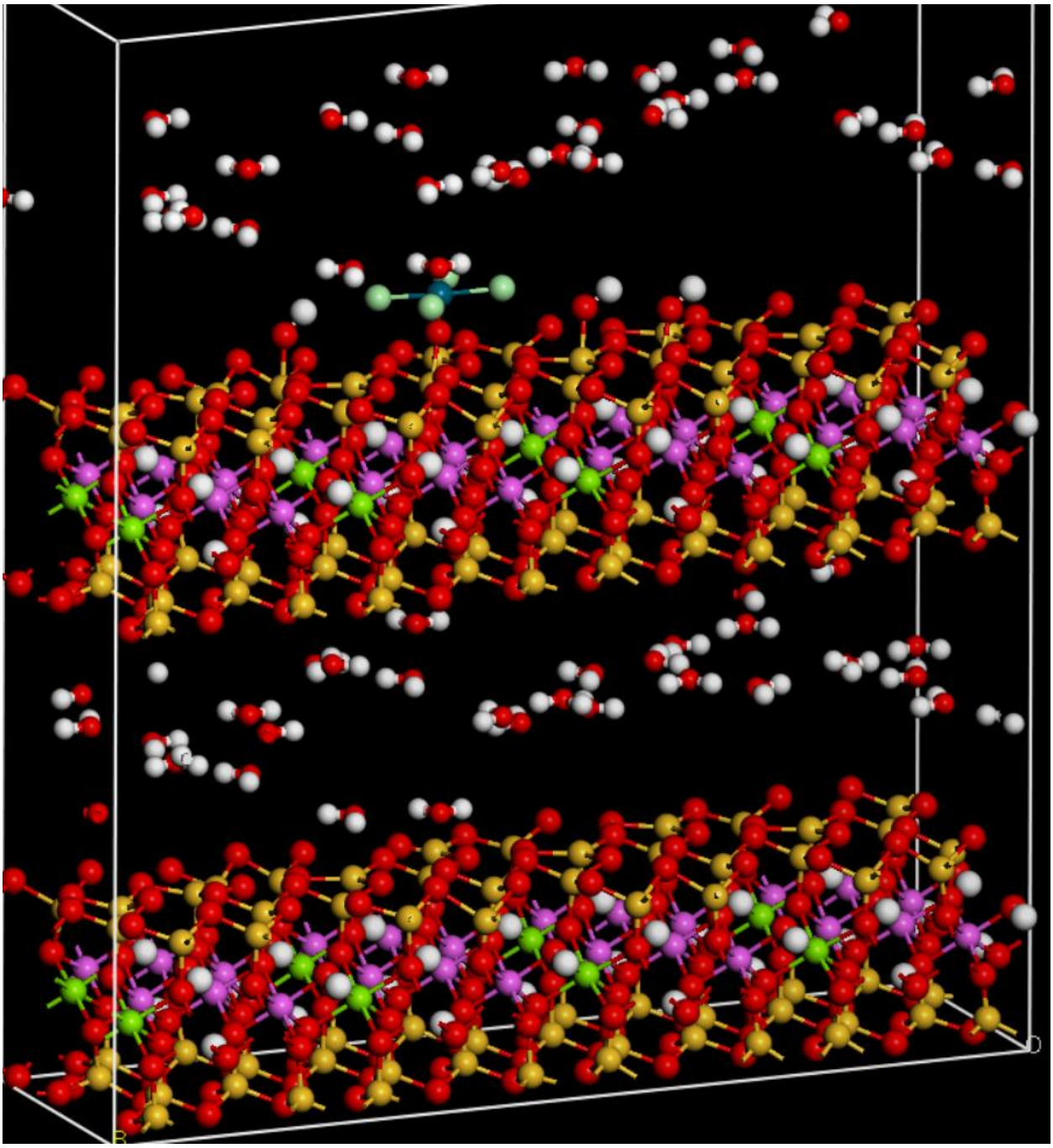

Figure 28 Sorption of $PdCl_4^{2-}$ on the Si sorption site of (001) montmorillonite surface

5. Discussion

5.1 Limitations of DFT

DFT is a powerful computational method and Materials Studio is a well-designed software that visualizes molecular structures for ease of use. However, there are still limitations. There has to be a trade-off between accuracy and time for DFT calculations. Although there are several settings that can be played around to let the software know whether accuracy of calculation or time of computation is being prioritized, all calculations except the series of calculations on the sorption of palladium-chloride species onto montmorillonite are done using lower accuracy settings. The computational time can be two to three times longer when using high accuracy settings compared to low accuracy settings.

DFT calculation only consumes CPU power, and there is a setting in the software for choosing how many cores of the CPU you want it to occupy. If all cores of the CPU were chosen, the device that is used to run the software would almost stop working but have the calculation run in the background. For less powerful devices such as a regular home PC or an office laptop, this might be fine if small models with less than 20 atoms were being calculated as the computing time would not be more than 30 to 40 minutes. However, computing time will rise exponentially as the model being computed gets larger and larger. The montmorillonite molecular structure has 420 atoms in one unit cell. The computing time for calculating the free

energy of it will be over 168 hours if the calculation runs on a normal home PC or an office laptop which typically has 2 to 4 cores in its CPU. This would mean that the device running the calculation will not be usable to do anything else for a whole week, which is very inconvenient when doing research and study. Even with a powerful CPU that has 24 to 32 cores, a complete calculation of the final state model of $PdCl^{+}$ sorption onto montmorillonite basal (001) surface silicon site, which has around 700 atoms, would take 24 to 48 hours. To give the device the ability to do basic functions such as browsing websites and writing a word document, at least 2 cores out of 24 or 32 need to be excluded from running the calculation. With limited time on the research, only the most important and complicated models that demand accuracy for results are calculated using the most cores and the most accurate settings.

Uncertainty and error analysis is also very hard in DFT calculations. Although the benchmark results in Section 4.1 showed the same positivity in sorption energies as the work from Puhakka et al. (2019), there are differences in the values of the sorption energies. The discrepancies are negligible because the output value from the DFT calculation is highly sensitive to changes in bond distances or atomic distances in general. A 10 picometer change in the distance between 2 atoms will change the free energy output from the DFT calculation, though the 10 picometer change is not significant enough to induce any meaningful change on the free energy output.

Another reason ties back to the dilemma of choosing between calculation accuracy and computational time. Less complex and important models take less time to compute, and more calculations can be run on the same model for uncertainty and error analysis. Unlike repeating the same experiments, repeating calculation on the same model does not require setting up from the beginning, and the output value would still change with calculations running on the same

settings. That means the accuracy of calculations will be the only significant influence on the uncertainty and error since the settings were adjusted to low accuracy for faster computational time.

On the other hand, more complex and important models take more time to run calculations with higher accuracy settings. However, the output value will not have a significant difference from one run to another on the same model because of the higher accuracy settings. Combined with the long computational time, it is not optimal to run a complex model multiple times when time is the limiting factor.

Therefore, taking into account the potential errors and uncertainties sources discussed, the conclusions are still reliable and do not require any further changes.

5.2 Materials Studio Constraints

In Materials Studio, there are many settings related to setting up a DFT calculation for a molecular model. However, the software is designed and implemented to calculate crystal structures. The calculation would not run at all if the molecular structure created was not included in a crystal structure. To fully utilize the software for DFT calculations, structures that are not originally crystal, such as a water molecule, must be included in a 3-D crystal unit cell frame to run a calculation on its free energy.

The cut-off energy mentioned in section 3 for setting up the simulations is one of the most important settings related to DFT calculations in Materials Studio. It is responsible for the convergence of the geometry optimization calculations that output the value of the model's free

energy in its simulated state. A calculation usually runs through a series of iterations to try to converge to a low energy state before starting to calculate the final free energy. If an error that says the calculation cannot converge occurred, the simulation would be halted and the following sequence of energy calculations would not take place at all. One of the only things that can be done to try to make the calculation converge is to adjust the value of the cut-off energy. However, the only way to determine whether the cut-off energy value needs to be adjusted higher or lower and by how much is by trial and error. There is no reliable way to know exactly what the value of cut-off energy needed to make the calculation converge and run successfully is. For small model calculations, the time it takes for the calculation to converge would be at most one hour. For large model calculations, sometimes 8 or 9 hours are needed for the calculation to converge.

6. Future Work

To continue with the research, the (010) surface of montmorillonite can be modelled and the sorption process between palladium-chloride species and potential sorption sites on the (010) surface should be investigated by calculating the sorption energies of palladium-chloride species on montmorillonite. This helps to fully investigate the sorption capability of montmorillonite.

To help with the post-closure safety assessment of the DGR, the sorption mechanism between palladium-chloride species and granite, which exists in the geological formation around the DGR. The sorption mechanism between other radionuclides of interest and montmorillonite or granite can be studied with DFT calculations. If there are experimental data that suggests the potential of sorption between such radionuclides and montmorillonite or granite, the DFT calculations could provide support and justification to the experimental data.

7. Conclusions

This study provides an in-depth analysis of the sorption behaviour of palladium onto montmorillonite in a saline environment using DFT simulations. The findings offer significant insights into the interactions and sorption mechanisms of palladium species in geological contexts.

Benchmark simulations confirmed the validity of the DFT approach, aligning well with previously established studies. By examining the free energies of all four palladium-chloride species $PdCl^{+}$, $PdCl_2$, $PdCl_3^{-}$, and $PdCl_4^{2-}$ in a Na-Ca-Cl saline environment, we identified their respective stabilities and potential to form under these conditions. The negative free energy values indicated the possibility of formation of these complexes, setting up a foundation for investigating the sorption energies of palladium-chloride species on montmorillonite surfaces.

Furthermore, the sorption energies of these palladium-chloride species on different montmorillonite surfaces were calculated. The sorption dynamics between palladium and montmorillonite in saline environment were investigated. Montmorillonite is an important mineral in bentonite clay which is one of the barriers within the deep geological repository. The calculated sorption energies using the DFT method reveal that surface complexation reactions take place between the montmorillonite surfaces and the palladium-chloride species in saline environment. The DFT calculations also show that $PdCl_4^{2-}$ is the most favourable species to sorb on the montmorillonite surfaces, followed by $PdCl_3^{-}$, $PdCl_2$ and $PdCl^{+}$. The result is consistent with the experimental data that the $PdCl_4^{2-}$ is the dominant sorbing species in saline solution.

Overall, the findings of this study are crucial for reassuring our understanding of the sorption behaviour of palladium in geological environments by providing a molecular-level perspective of the palladium-chloride species and montmorillonite models.

8. References

Adamis, Z., & Williams, R. B. (2005). *Bentonite, kaolin, and selected Clay Minerals*. World Health Organization.

Atkins, P., & De Paula, J. (2010). *Physical Chemistry* (9th ed.). Oxford University Press.

Bradbury, M. H., & Baeyens, B. (2005). Experimental and modelling studies on the sorption of Cs, Sr, Ni, Eu, Th, Sn, and U on montmorillonite. *Geochimica et Cosmochimica Acta*, 69(22), 5403-5412.

Choppin, G. R., Rao, L., & Morgenstern, A. (2002). Complexation of palladium(II) with chloride in aqueous solution. *Radiochimica Acta*, 90(9-11), 677-682.

Churchman, G. J. (2002). Formation of complexes between bentonite and organic compounds. In *Applied Clay Science* (Vol. 21, pp. 177-189). Elsevier.

Chutia, P., Kato, S., Kojima, T., & Satokawa, S. (2009). Adsorption of As(V) on surfactant-modified natural zeolites. *Journal of Hazardous Materials*, 162(1), 204-211.

Clark, S. J., Segall, M. D., Pickard, C. J., Hasnip, P. J., Probert, M. I., Refson, K., & Payne, M. C. (2005). First principles methods using CASTEP. *Zeitschrift Für Kristallographie - Crystalline Materials, 220(5–6),* 567–570.

Clever, H. L., & Johnston, F. J. (1979). The solubility of some sparingly soluble salts of zinc and cadmium in water and in aqueous electrolyte solutions. *Journal of Physical and Chemical Reference Data*, 8(2), 289-422.

Colàs, E., Valls, A., García, D., & Duro, L. (2021). *Radionuclide solubility calculation (Phase 1)* (Nuclear Waste Management Organization Technical Report NWMO-2021-02). Toronto, Canada.

Colàs, E., Valls, A., García, D., & Duro, L. (2022). *Radionuclide solubility calculation (Phase 2)* (Nuclear Waste Management Organization Technical Report NWMO-2022-11). Toronto, Canada.

Du, J., Wang, Q., & Chen, J. (2022). Understanding Cd^{2+} adsorption mechanism on montmorillonite surfaces by combining DFT and MD. *Processes, 10*(7), 1381.

Ewing, R. C. (2015). Long-term storage of spent nuclear fuel. *Nature Materials,* 14(3), 252-257.

Goguen, J., Walker, A., Racette, J., Riddoch, J., & Nagasaki, S. (2021). Sorption of Pd on illite, MX-80 bentonite and shale in Na–Ca–Cl Solutions. Nuclear Engineering and Technology, 53(3), 894–900.

Hastings, I. J., Radde, E., & Carbol, P. (2018). CANDU fuel: An overview. *Journal of Nuclear Materials*, 506, 105-112.

Hinz, C. (2001). Description of sorption data with isotherm equations. *Geoderma, 99*(3-4), 225-243.

Hohenberg, P., & Kohn, W. (1964). Inhomogeneous electron gas. *Physical Review, 136*(3B), B864.

International Atomic Energy Agency (IAEA). (2003). *Management of spent fuel from nuclear power reactors: An overview of the IAEA's activities*.

Karnland, O. (2010). Chemical and mineralogical characterization of the bentonite buffer for the acceptance control procedure in a KBS-3 repository. *SKB Technical Report*, 10-60.

Knief, R. A. (2014). *Nuclear engineering: Theory and technology of commercial nuclear power* (3rd ed.). American Nuclear Society.

Kragten, J. (1980). An evaluation of the stability constants of the Chloro-complexes of palladium(ii). *Talanta, 27*(4), 375–377.

Kresse, G., & Furthmüller, J. (1996). Efficient iterative schemes for ab initio total-energy calculations using a plane-wave basis set. *Physical Review B, 54*(11), 11169-11186.

Leach, A. R. (2001). *Molecular modelling: Principles and applications*. Prentice Hall.

Li, X., He, J., Zhang, Y., Zhang, G., & Wang, H. (2012). Adsorption of Hg^{2+} on TiO_2 surfaces: A density functional theory study. *Journal of Hazardous Materials, 243*, 404-410.

Li, Z., Shuang, C., & Zhang, Y. (2013). Sorption of palladium(II) on montmorillonite: Effects of pH, ionic strength, foreign ions, humic substances, and temperature. *Journal of Radioanalytical and Nuclear Chemistry*, 298(1), 35-44.

Lu, C., Chung, Y.-L., & Chang, K.-F. (2006). Adsorption of heavy metals by CNT composites. *Journal of Physical Chemistry B, 110*, 24313-24320.

Ma, W., Xu, Z., & Wang, L. (2010). Sorption of Pd(II) from aqueous solution onto Fe_3O_4/graphene nanocomposites. *Chemical Engineering Journal*, 198-199, 71-79.

Martin, R. M. (2004). *Electronic Structure: Basic Theory and Practical Methods*. Cambridge University Press.

Metz, V., Geckeis, H., González-Robles, E., Loida, A., Bube, C., & Kienzler, B. (2012). Radionuclide behaviour in the near-field of a geological repository for spent nuclear fuel. *Radiochimica Acta, 100*(8–9), 699–713.

Murray, H. H. (2007). Applied Clay Mineralogy. *Developments in Clay Science* (Vol. 2). Elsevier.

Nagasaki, S., & Nakayama, S. (2015). *Radioactive Waste Engineering and Management*. Springer.

Nagasaki, S., Riddoch, J., & Racette, J. (2019). Contribution of ternary reaction to Pd sorption on MX-80 in Na-Ca-Cl solution at high ionic strength. *Science and Technology of Nuclear Installations*, 2019, 1-6.

Naserifard, N., Lee, A., Birch, K., Chiu, A., & Zhang, X. (2021). *Deep geological repository conceptual design report crystalline/sedimentary rock* (Nuclear Waste

Management Organization-Adaptive Phase Management-Report-00440-0211-R000). Toronto, Canada.

Novoselov, K. S., Geim, A. K., Morozov, S. V., Jiang, D., Zhang, Y., Dubonos, S. V., Grigorieva, I. V., & Firsov, A. A. (2004). Electric field effect in atomically thin carbon films. *Science, 306*(5696), 666-669.

Nuclear Waste Management Organization. (2017). Postclosure safety assessment of a used fuel repository in crystalline rock. *Nuclear Waste Management Organization Technical Report NWMO TR-2017-02*.

Nuclear Waste Management Organization. (2018). Postclosure safety assessment of a used fuel repository in sedimentary rock. *Nuclear Waste Management Organization Technical Report NWMO TR-2018-08*.

Nuclear Waste Management Organization. (2022). *Nuclear Fuel Waste Projections in Canada – 2022 Update*.

Payne, M. C., Teter, M. P., Allan, D. C., Arias, T. A., & Joannopoulos, J. D. (1992). Iterative minimization techniques for ab initio total-energy calculations: molecular dynamics and conjugate gradients. *Reviews of Modern Physics, 64*(4), 1045-1097.

Park, M. B., Lee, C. S., & Shin, W. H. (2010). Density functional theory study on the adsorption of Pb^{2+} and Cd^{2+} on zeolites. *Journal of Physical Chemistry C, 114*, 2471-2480.

Puhakka, E., Li, X., Ikonen, J., & Siitari-Kauppi, M. (2019). Sorption of selenium species onto phlogopite and calcite surfaces: DFT Studies. *Journal of Contaminant Hydrology*, *227*, 103553.

Pusch, R. (2001). The buffer and backfill handbook. Part 2: Materials and techniques. *SKB Technical Report*, 02-12.

Santos, E. J. G., Ayala, P., Zhu, J., Ajayan, P. M., & Rümmeli, M. H. (2016). Electronic and catalytic properties of boron nitride nanomaterials. *Nanoscale*, *8*(12), 6057-6072.

Sharma, P., Kaur, J., & Mittal, S. K. (2017). Removal of palladium(II) from aqueous solutions using low-cost adsorbents: A comparative study. *Journal of Environmental Chemical Engineering*, 5(3), 3004-3014.

Sposito, G. (1984). *The Surface Chemistry of Soils*. Oxford University Press.

Stumm, W. (1992). *Chemistry of the Solid-Water Interface: Processes at the Mineral-Water and Particle-Water Interface in Natural Systems*. John Wiley & Sons.

Stumm, W., & Morgan, J. J. (1996). *Aquatic Chemistry: Chemical Equilibria and Rates in Natural Waters* (3rd ed.). New York: John Wiley & Sons, Inc.

Sundaram, A. K., & Sandell, E. B. (1955). Chloro complexes of palladium(ii) in solution. *Journal of the American Chemical Society*, *77*(4), 855–857.

Van, H. T., Glaus, M. A., & Van Loon, L. R. (2001). The interaction of Nd(III) and Th(IV) with humic substances: Complexation and sorption onto kaolinite. *Radiochimica Acta*, 89(8), 493-499.

Wieland, E., Hummel, W., & Van Loon, L. R. (2006). The influence of complexing ligands on the sorption of Eu(III) and Th(IV) on montmorillonite: A comparison with linear free energy relationships. *Radiochimica Acta*, 94(6-7), 431-439.

Zhao, J., Ren, W., Cheng, H.-M., & Gao, C. (2011). Adsorption of heavy metal ions by graphene oxide: A density functional theory study. *Environmental Science & Technology*, *45*, 10454-10462.

Zhao, W., & Xue, Q. (2020). Recent advances in the applications of two-dimensional graphene and its derivatives in organic light-emitting diodes. *Journal of Materials Chemistry C*, *8*(22), 7606-7618.

Zoveidavianpoor, M. (2018). *Current topics in the utilization of clay in industrial and medical applications Mansoor Zoveidavianpoor*. IntechOpen.